RADAR PROPAGATION MODELLING USING THE SPLIT STEP PARABOLIC EQUATION METHOD

A THESIS SUBMITTED TO
THE GRADUATE SCHOOL OF NATURAL AND APPLIED SCIENCES
OF
THE MIDDLE EAST TECHNICAL UNIVERSITY

BY

ALPASLAN TÜRKBOYLARI

IN PARTIAL FULFILLMENT OF THE REQUIREMENTS FOR THE DEGREE OF

MASTER OF SCIENCE

IN

THE DEPARTMENT OF ELECTRICAL AND ELECTRONIC ENGINEERING

JANUARY 2004

Approval of the Graduate School of Natural and Applied Sciences.

Prof. Dr. Canan Özgen
Director

I certify that this thesis satisfies all the requirements as a thesis for the degree of Master of Science.

Prof. Dr. Mübeccel Demirekler
Head of Department

This is to certify that we have read this thesis and that in our opinion it is fully adequate, in scope and quality, as a thesis for the degree of Master of Science.

Assoc. Prof. Dr. Seyit Sencer Koç
Supervisor

Examining Committee Members

Prof. Dr. Altunkan Hızal

Prof. Dr. Fatih Canatan

Prof. Dr. Nilgün Günalp

Assoc. Prof. Dr. Seyit Sencer Koç

M. S. Eng. Orhan Şengül

ABSTRACT

RADAR PROPAGATION MODELLING USING THE SPLIT STEP PARABOLIC EQUATION METHOD

Türkboyları, Alpaslan
M.S., Department of Electrical and Electronic Engineering
Supervisor: Assoc. Prof. Dr. Seyit Sencer Koç

January 2004, 50 pages

This document describes radar propagation modelling using split step parabolic wave equation (PWE) method. A computer program using Fourier split-step (FSS) marching technique is developed for predicting the electromagnetic wave propagation in troposphere. The program allows specification of frequency, polarization, antenna radiation pattern, antenna altitude, elevation angle and terrain profile. Both staircase terrain modelling and conformal mapping are used to model the irregular terrain. Mixed Fourier transform is used to implement the impedance boundary conditions. The conditions and the limits of different approximations are stated. The propagation code, RPPT (Radar Propagation Prediction Tool) is developed in Matlab 6.0 with a user friendly GUI. Different PWE methods can be selected in RPPT for different applications. The results are presented as one-way propagation factor and path loss in decibels versus range. Comparisons are made between different PWE techniques and other propagation models to demonstrate the ability and accuracy of the present model to accommodate various situations. It is assumed that the reader is familiar with the tropospheric propagation.

Keywords: Radar Simulation, Propagation, Parabolic Wave Equation, Split-Step Fourier Transform

ÖZ

AYRIK BASAMAK PARABOLİK DALGA DENKLEMİ KULLANARAK RADAR PROPAGASYON MODELLEMESİ

Türkboyları, Alpaslan
Yüksek Lisans, Elektrik ve Elektronik Mühendisliği Bölümü
Tez Yöneticisi: Assoc. Prof. Dr. Seyit Sencer Koç

Ocak 2004, 50 sayfa

Bu doküman ayrık basamaklı parabolik dalga denklemini (PDD) kullanarak radar propagasyonu modellenmesini tanıtmaktadır. Troposferdeki elektromanyetik dalga propagasyonunu kestirmek için Ayrık Basamaklı Fourier (ABF) dönüşüm tekniğini kullanan bir bilgisayar program geliştirildi. Frekans, polarizasyon, anten yayılım paterni, anten yüksekliği, irtifa açısı ve arazi şekli parametrelerini modele girmek mümkün olmaktadır. Düzensiz arazi şekillerini modellemek için; merdiven arazi ve uyumlu haritalama yöntemleri kullanılmıştır. Sınır empedans şartlarını sağlamak için karma Fourier dönüşümü (KFD) kullanıldı. Yapılan farklı yuvarlamaların sınırları ve şartları ifade edilmiştir. Kullanışlı bir arayüze sahip olan propagasyon modeli, RPPT (Radar Propagasyon Kestirim Aracı) Matlab 6.0'da geliştirilmiştir. RPPT'de farklı uygulamalar için farklı PDD teknikleri seçilebilmektedir. Sonuçlar, tek-yol propagasyon faktörü ve yol kaybı desibel cinsinden mesafeye bağlı olarak gösterilmektedir. Modelin farklı durumları ele alabilme kabiliyetine ve hassasiyetine sahip olduğunu göstermek için, farklı PDD teknikleri ve propagasyon modelleri arasında karşılaştırmalar yapılmıştır. Okuyucunun tro-

posferik propagasyon hakkında genel bilgi sahibi olduğu varsayılmıştır.

Anahtar Kelimeler: Radar Simülasyonu, Propagasyon, Parabolik Dalga Denklemi, Ayrık Basamaklı Fourier Dönüşüm

ACKNOWLEDGMENTS

First of all, I would like to thank my supervisor Assoc. Prof. Dr. S.Sencer Koç for his encouragement and support throughout the development of this thesis. I am also in great dept to Orhan Şengül for providing RADCAL software outputs included in this thesis.

Turkish Air Force is appreciated for the utilization of the computer based recourses.

I am especially grateful to my parents for their support and encouragement.

TABLE OF CONTENTS

ABSTRACT iii

ÖZ v

ACKNOWLEDGMENTS vii

TABLE OF CONTENTS viii

LIST OF TABLES xi

LIST OF FIGURES xii

CHAPTER

I INTRODUCTION 1

I.1 Problem Description 1

I.2 Scope And Objective 3

I.3 Outline 4

II THEORY OF THE PARABOLIC WAVE EQUATION 5

II.1 General Theory 5

II.2 Derivation of Parabolic Wave Equation 6

II.3 Split-Step Fourier Solution of the PWE 7

II.4 Split-Step Sine Transform Solution of the PWE 9

II.5 Split-Step Fourier Solution of the WAPWE 9

II.6 Mixed Fourier Solution of the WAPWE 10

II.7 Boundary Conditions 11

II.7.1 The Upper Boundary Condition 11

II.7.2 The Surface Boundary Condition 11

II.7.2.1 Dirichlet Boundary Condition 12

II.7.2.2 Neumann Boundary Condition 12

II.7.2.3 Leontovich Boundary Condition . . . 13

II.7.3 Reflection Coefficient 13
II.8 Irregular Terrain Modelling 15
II.8.1 Staircase Terrain Modelling 15
II.8.2 Conformal Mapping 15
III SIMULATION RESULTS 17
III.1 General Description 17
III.2 Results Of Different Approaches 20
III.2.1 Variation of FFT size and time (100MHz, 1GHz, 3GHz) 21
III.2.2 Variation of Maximum Propagation Angle with SPWE and WAPWE 22
III.2.3 Horizontal versus Vertical Polarization with WAPWE 22
III.2.4 Flat Earth and Flattened Earth Models with SPWE 24
III.2.5 Staircase versus Conformal Mapping with SPWE (Rectangle, Pyramid, Sinuson, Sinusoidal) 25
III.2.6 Ground Wave Propagation with WAPWE 27
III.3 Comparison With CARPET 29
III.4 Comparison With RADCAL 32
IV CONCLUSION AND FUTURE WORK 37
IV.1 Conclusion 37
IV.2 Future Work 38
REFERENCES 38
APPENDICES 42
A PROPAGATION FACTOR AND PATH LOSS 42
B FFT PARAMETERS 43
C SOURCE MODELLING 44
D TERRAIN FUNCTIONS 45
D.1 Rectangle Hill 45
D.2 Pyramid Hill 45
D.3 Sinuson Hill 46
D.4 Sinusoidal Surface 46

E REFRACTIVITY PROFILES 47
E.1 Evaporation Duct 48
E.2 Surface Based Duct 49
E.3 Elevated Duct 49
E.4 Earth Flattening Transformation 49

LIST OF TABLES

II.1 Surface Medium Characteristics 14

III.1 FFT Size and Time for SPWE. 21

LIST OF FIGURES

II.1 Range-Marching Technique 8

III.1 Radar Propagation Prediction Tool (RPPT) Main Window. . . . 18
III.2 Propagation Model Settings Window. 18
III.3 Surface Based Duct with SPWE. 19
III.4 SPWE and Analytic data. 21
III.5 Horizontally Polarized Wave Propagation. 23
III.6 Vertically Polarized Wave Propagation. 23
III.7 Flat Earth (a) and Flattened Earth (b) Models. 24
III.8 Rectangle Hill with Staircase (a) versus Conformal (b) Mapping. . 25
III.9 Sinuson Hill with Staircase (a) versus Conformal (b) Mapping. . . 26
III.10 Pyramid Hill with Staircase (a) versus Conformal (b) Mapping. . 26
III.11 Sinusoidal Hill with Staircase (a) versus Conformal (b) Mapping. 26
III.12 Ground Wave Propagation with SPWE. 28
III.13 Ground Wave Propagation with WAPWE. 28
III.14 CARPET (a) vs RPPT (b) output at 100 Mhz. 30
III.15 CARPET (a) vs RPPT (b) output at 1 GHz. 30
III.16 CARPET (a) vs RPPT (b) output at 3 GHz. 31
III.17 CARPET Settings. 31
III.18 RADCAL output at 1 GHz over flattened Earth. 32
III.19 RPPT output at 1 GHz over flattened Earth. 33
III.20 RADCAL output over a hill below LOS. 34
III.21 RPPT output over a sinuson hill below LOS. 34
III.22 RADCAL output over a hill obscuring LOS. 35
III.23 RPPT output over a sinuson hill obscuring LOS. 35
III.24 RADCAL Hills with 100 m (a) and 229 m (b) height. 36

CHAPTER I

INTRODUCTION

I.1 Problem Description

RADAR (RAdio Detection And Ranging) is an electromagnetic system which is used in a wide variety of applications including defense, air traffic control, meteorology, and mapping. The basic idea behind radar is to transmit a particular type of waveform and analyze the echo signal. With the unavoidable presence of various types of interference, signal processing is naturally an important part of any radar system. The usual parameters extracted from an echo signal can be range, radial velocity and angular position of a target. While analyzing radar performance, the earth's surface and the medium in which radar waves propagate should be taken into account. Rigorous modelling of the interaction of electromagnetic (EM) waves with natural and man-made bodies and surfaces is the cornerstone of many important military and civilian applications. The prediction of propagation factor at low grazing angles over terrain is a critical area for numerical modelling and performance.

Different computational techniques are used for the prediction of propagation factor such as the ray tracing approach, the parabolic equation approach, and the integral equation approach. The Parabolic Wave Equation (PWE) is a forward scatter approximation to the full Helmholtz wave equation and inherently includes effects due to spherical-Earth diffraction, atmospheric refraction, and surface re-

flections (i.e. multipath). Advanced PWE models may also include impedance boundaries, rough surfaces, complicated antenna patterns, irregular terrain, atmospheric absorption and surface waves. It is known to be a numerically efficient method to model tropospheric radiowave propagation over irregular terrain in the presence of range-dependent nonstandard environmental conditions. The PWE can be implemented by using Fourier split-step (FSS) method or implicit finite difference (IFD) method. IFD method allows straightforward implementation of complex boundaries, while FSS is numerically more stable. The optimal choice of solution method is done according to the application. To include wide angles of propagation over terrain Wide-Angle Parabolic Wave Equation (WAPWE) is used.

The PWE was first derived by Fock in the 1940's, [1]. Leontovich and Fock introduced the parabolic approximation for very simple atmospheric and surface boundary conditions. Hardin and Tappert introduced an efficient numerical approach for solving the PWE called Fourier split-step algorithm in 1973. Tappert used FSS technique to solve the acoustic PWE numerically in 1977, [2]. Harvey Ko and colleagues in APL's (Applied Physics Laboratory) Submarine Technology Department (STD) modified the acoustic model to address electromagnetic propagation in the troposphere in 1981. Beilis and Tappert developed a general coordinate transformation that flattens the undulating surface to account for irregular surface effects in 1979, [3]. McArthur and Bebbington subsequently investigated tilting or steering the field to counteract the flattening of the surface without an explicit coordinate transformation in 1991. In another approach, Dozier used a local or piecewise conformal mapping to locally flatten the surface in 1984, [4]. Kuttler and Dockery developed the mixed Fourier Transform method to accommodate a finitely conducting dielectric boundary in the FSS solution in 1991, [5, 6]. By comparing the PWE propagation predictions in the forward direction to those based on geometrical optics, they confirmed the accuracy of the PWE model for predominant forward propagation. The development of the wide-angle parabolic wave equation (WAPWE) method is attributed to different authors, Claerbout in 1985, Greene in 1984 and Collins in 1989 who proposed

different models.

Barrios developed a model called TPEM (Terrain Parabolic Equation Model) which uses the original Beilis/Tappert approach on a variety of sample terrain problems, [7]. The SPAWAR Systems Center at San Diego (SSC-SD) has developed Advanced Refractive Effects Prediction System (AREPS) program, [8]. At the core of AREPS is Advanced Propagation Model (APM) which is a hybrid ray-optic and parabolic equation (PE) model that uses the complementary strengths of both methods to construct a fast and accurate composite model. The Theater Systems Development Group of APL's Air Defense Systems Department has developed the computational model TEMPER (Tropospheric Electromagnetic Parabolic Equation Routine) to accurately calculate electromagnetic propagation over the sea in complicated refractive environments. M.Cayer has developed the PE-LRTS software using the FSS PWE algorithm for representing electromagnetic wave propagation at low-level over the sea in 1995.

I.2 Scope And Objective

In this thesis, the main objective is to model tropospheric radiowave propagation over irregular terrain. The propagation model, RPPT (Radar Propagation Prediction Tool) is based on the 2D FSS solution of the PWE. Both staircase terrain modelling and conformal mapping are used to model the irregular terrain. The computational domain is doubled and an "image atmosphere" is used to account for perfectly conducting surfaces. To accommodate finitely conducting surfaces, the mixed Fourier transform (MFT) is used. Some of the approximations and resulting errors that are encountered in the model are addressed. The errors in the algorithm are minimized by appropriate selection of variables. The conditions and the limits of different approximations are stated. The comparison of RPPT with different models are available, but it was not possible to compare with measured data. The comparisons showed agreement between different models.

RPPT is developed in Matlab 6.0 with a user friendly GUI. The screens of the program and the way of using it is explained. But, to modify some of the parameters of the model, the Matlab code should be edited with the guidance of

the comments included in the code. Later, this code could be rewritten in C++ and could be a part of a hybrid model.

I.3 Outline

Chapter II begins with the derivation of the parabolic wave equation and its numerical solution via the Fourier split-step marching technique. The Sine Transform Solution of PWE and Mixed Fourier Transform Solution of WAPWE along with a detailed account of the underlying assumptions and approximations can be found in Chapter II. The solution of the PWE is extended to accommodate Dirichlet, Neumann and Leontovich boundary conditions with irregular terrain.

In Chapter III, Matlab simulation results are compared with different models such as CARPET and RADCAL. During comparison, various parameters like frequency, beamwidth, antenna height, terrain and atmospheric conditions are taken into account. The performance of the PWE with different FSS algorithms is evaluated in Chapter III.

Finally, The Conclusion and Future Work are given in Chapter IV.

CHAPTER II

THEORY OF THE PARABOLIC WAVE EQUATION

II.1 General Theory

As a second-order equation, the Maxwell equations are hyperbolic. Thus a generic numerical solution will not be suitable. One should use Fourier series-based methods or some other method which can handle hyperbolic behavior. Assuming azimuthal symmetry, Maxwell's equations can be reduced to a two-dimensional scalar Helmholtz equation. The Helmholtz equation is then factored into forward and backward propagating pieces. We use a parabolic approximation of the scalar wave equation by neglecting the backscattered wave energy. The scalar form of the Helmholtz wave equation corresponds to one component of the vector electric or magnetic field. The main advantage of the PWE is that it can be solved as an initial value problem in range (x) using range-marching techniques for a given source-field distribution over the height (z) at the initial range. The FSS algorithm is an important one of these marching techniques that has been used extensively to solve the standard PWE. The FSS method is exact for homogeneous unbounded media and approximate for inhomogeneous unbounded media. MFT is a rigorous method to accurately represent electromagnetic propagation over an impedance boundary. The PWE approximation neglects backscatter and its accuracy deteriorates for off-horizontal propagation. In addition, as mandated by

the errors associated with the FSS algorithm, the medium under consideration should also be slowly varying. When using discrete transforms, the maximum propagation angle, $p_{\max}$, is related to the transform size, frequency and $z_{\max}$ according to the Nyquist criterion. Both z space and p space are band limited to accommodate a finite transform size. The transform size is directly proportional to frequency and propagation angle. (See Appendix B) To prevent strong reflections from the nonphysical upper boundary, the PWE solution field strength is smoothly attenuated by using Hanning window.

II.2 Derivation of Parabolic Wave Equation

We start with the three-dimensional scalar Helmholtz wave equation for an electric or magnetic field component ψ:

$$\nabla^2\psi + k^2n^2\psi = 0 \tag{II.1}$$

where $k_0 = \frac{2\pi}{\lambda}$ is the free space wave number and n is the refractive index. The analysis is greatly simplified by applying the usual earth flatting formulation that allows us to express the wave equation in cylindrical (two-dimensional) coordinates and assuming the azimuthal symmetry about the vertical axis through the radar. In two dimensional space, each scalar component of the electromagnetic field, ψ, is governed by the scalar wave equation :

$$\frac{\partial^2\psi}{\partial z^2} + \frac{\partial^2\psi}{\partial x^2} + \frac{1}{x}\frac{\partial\psi}{\partial x} + k_0^2n^2\psi = 0 \tag{II.2}$$

where x and z are the horizontal (range) and vertical (altitude) coordinates. When we work with cylindrical coordinates (x, z, θ) and assume azimuthal symmetry about the vertical axis, the function ψ corresponds to H_θ for vertical polarization and E_θ for horizontal polarization. To obtain the Parabolic Wave Equation, we first assume that the field ψ propagates as time-harmonic (e^{-jwt}), and cylindrical of the form $\psi(x, z) = \frac{e^{jkx}}{\sqrt{kx}}u(x, z)$. This implies that u varies slowly at angles close to paraxial direction (preferred direction of computation) (Fig.II.1). After substitution of $u(x, z)$ into the Eqn.II.2, the wave equation becomes:

$$\frac{\partial^2u}{\partial z^2} + \frac{\partial^2u}{\partial x^2} + 2jk\frac{\partial u}{\partial x} + k^2\left[n^2(x, z) - 1 + \frac{1}{(2kx)^2}\right]u = 0. \tag{II.3}$$

We can drop the $\frac{1}{(2kx)^2}$ term after making the far-field assumption, $kx \gg 1$. Assuming $\left|\frac{\partial^2 u}{\partial x^2}\right| \ll 2k\left|\frac{\partial u}{\partial x}\right|$ (The Paraxial approximation) because of the slow variation of u, Eqn.II.3 reduces to the Standard Parabolic Wave Equation :

$$\frac{\partial^2 u}{\partial z^2} + 2jk\frac{\partial u}{\partial x} + k^2\left[n^2(x,z) - 1\right]u = 0. \tag{II.4}$$

II.3 Split-Step Fourier Solution of the PWE

Rewriting the above Standard Parabolic Wave Equation after taking the Fourier transform of both sides, assuming that the refractive index $n(x,z)$ is constant, the following can be obtained:

$$\frac{\partial U(x,p)}{\partial x} = \left(\frac{-jp^2}{2k} + \frac{jk\left[n^2(x,z) - 1\right]}{2}\right)U(x,p) \tag{II.5}$$

with $U(x,p) = \mathcal{F}\{u(x,z)\}$. The transform variable p is a function of the propagation angle θ: $p = k\sin\theta$ where θ is the angle relative to the horizontal. Recall that the Fourier transform of a derivative is jp times the transform. The solution of Eqn.II.5 can be expressed as:

$$U(x,p) = U(0,p) \times e^{j\left(\frac{-p^2}{2k} + \frac{k\left[n^2(x,z)-1\right]}{2}\right)x} \tag{II.6}$$

where $U(0,p)$ is the given source function on the z axis. The Fourier Split-Step Solution of the PWE can be obtained after taking the inverse Fourier transform of Eqn.II.6 and writing the solution at range $x + \Delta x$:

$$u(x + \triangle x, z) = e^{\frac{jk\triangle x\left(n^2(x,z)-1\right)}{2}}\mathcal{F}^{-1}\left[e^{\frac{-j\triangle x p^2}{2k}}\mathcal{F}(u(x,z))\right] \tag{II.7}$$

where $\mathcal{F}$ and $\mathcal{F}^{-1}$ are the forward and inverse Fourier transforms in (z,p) space. The Fourier transforms $\mathcal{F}$ and $\mathcal{F}^{-1}$ are defined by

$$\begin{aligned} U(x,p) &= \mathcal{F}[u(x,z)] = \int_{-\infty}^{+\infty} u(x,z)\, e^{-jpz}dz \\ u(x,z) &= \mathcal{F}^{-1}[U(x,p)] = \frac{1}{2\pi}\int_{-\infty}^{+\infty} U(x,p)e^{jpz}dp. \end{aligned} \tag{II.8}$$

The FSS method, makes use of Fourier Transforms to implement a range-marching technique as shown in Fig.II.1. This solution is exact when $n(x,z)$ does

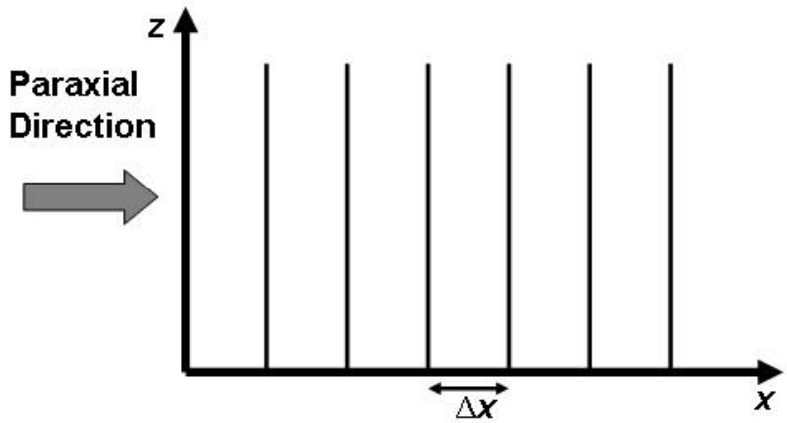

Figure II.1: Range-Marching Technique

not change with z, which effectively corresponds to propagation in an infinite, homogeneous medium. The exponential term $n^2(x,z)-1$ can be replaced by the modified refractivity, $m(x,z)$. To take into account the earth's curvature, $m(x,z)$ is defined by $m(x,z)=\left\{\left[n(x,z)+\frac{z}{a}\right]^2-1\right\}$ where a is the earth's radius, [6, 9, 5]. When effective radius of the Earth $\left(a_e=\frac{4}{3}\times a\right)$, is used, the standard atmosphere condition is included in the computations, [15]. Assuming $\left(\frac{z}{a}\right)^2 \ll 1$, m can be expressed as $\left[n^2(x,z)-1+\frac{2z}{a}\right]$. We can further approximate $n^2(x,z)-1$ by $2(n(x,z)-1)$, because $(n^2(x,z)-1)\ll 1$ in usual atmospheric conditions, [10]. Thus, the approximations can be summarized as,

$$\left[n(x,z)+\frac{z}{a}\right]^2-1 \cong n^2(x,z)-1+\frac{2z}{a} \cong 2\left[n(x,z)-1+\frac{z}{a}\right]. \tag{II.9}$$

The earth's curvature enters only through the $\frac{2z}{a}$ term, and this term is ignored for propagation over a flat earth. The approximations can be expressed as

$$\begin{aligned} n^2(x,z)-1 &\cong 2N(x,z)\times 10^{-6} \\ \left[n(x,z)+\frac{z}{a}\right]^2-1 &\cong 2M(x,z)\times 10^{-6} \end{aligned} \tag{II.10}$$

in terms of $N(x,z)$ and $M(x,z)$ defined in E.2 and E.5 respectively. In realistic cases, however, $n(x,z)$ is a slowly varying function of z and often x as well, and therefore there are errors associated with the Split-Step Fourier Solution of the PWE. Practically, these errors limit the range step size $\triangle x$. Fourier Split Step (FSS) solution marches the solution forward from x to $x+\triangle x$. The FSS solution

of PWE gives accurate results at angles up to nearly $\pm 15°$, [11, 12], and is straight forward to implement on a computer.

II.4 Split-Step Sine Transform Solution of the PWE

For a smooth, perfectly conducting surface, the boundary condition is $u(x,z) = 0$ for horizontal polarization and $\frac{\partial u}{\partial z} = 0$ at $z = 0$ for vertical polarization. In these cases the Fourier transform can be represented by a one-sided sine or cosine transform. Then the split step solution of Eqn.II.4 is

$$u(x + \triangle x, z) = e^{\frac{jk\triangle x m(x,z)}{2}} \mathcal{F}_s^{-1}\left[e^{\frac{-j\triangle x p^2}{2k}} \mathcal{F}_s\left(u(x,z)\right)\right] \tag{II.11}$$

where $\mathcal{F}_s$ and $\mathcal{F}_s^{-1}$ are the forward and inverse Fourier sine transforms in (z,p) space, [5]. The Fourier sine transform $\mathcal{F}_s$ is defined by

$$U(x,p) = \mathcal{F}_s\left[u(x,z)\right] = -2j\int_0^{+\infty} u(x,z)\sin(pz)\,dz \tag{II.12}$$

and the Fourier inverse sine transform $\mathcal{F}_s^{-1}$ is defined by

$$u(x,z) = \mathcal{F}_s^{-1}\left[U(x,p)\right] = \frac{j}{\pi}\int_0^{+\infty} U(x,p)\sin(pz)\,dp. \tag{II.13}$$

II.5 Split-Step Fourier Solution of the WAPWE

We rewrite the scalar Helmholtz wave equation using cylindrical (two-dimensional) coordinates in the following operator form

$$\left[P^2 + k^2 Q^2\right] u(x,z) = 0 \tag{II.14}$$

where $P = \frac{\partial}{\partial x}$. The pseudo-differential operator Q is defined as:

$$Q = \left(\frac{1}{k^2}\frac{\partial^2}{\partial z^2} + n^2(x,z)\right)^{1/2}. \tag{II.15}$$

After factoring Eqn.II.14 and considering the forward wave equation we obtain

$$Pu(x,z) = -jkQu(x,z). \tag{II.16}$$

An approximation to Q assumes that the variations of the refractive index are small, i.e. $(n^2(x,z) - 1) \ll 1$. Let us introduce the following abbreviation

$$q = \left(\frac{1}{k^2}\frac{\partial^2}{\partial z^2} + n^2(x,z) - 1\right). \tag{II.17}$$

By expanding Q using Taylor series, we may then write

$$Q = \sqrt{1+q} = 1 + \frac{q}{2} - \frac{q^2}{8} + ... \tag{II.18}$$

By keeping only the first two terms in the above series, Q can be rewritten in the following form

$$Q \cong \left(1 + \frac{1}{k^2}\frac{\partial^2}{\partial z^2}\right)^{1/2} + \frac{(n^2(x,z)-1)}{2}. \tag{II.19}$$

After substituting Eqn.II.19 into Eqn.II.16 we obtain the FSS solution of WAPWE as

$$u\left(x+\triangle x, z\right) = e^{\frac{jk\triangle x m(x,z)}{2}} \mathcal{F}^{-1}\left[e^{-j\triangle x\left(k-\sqrt{k^2-p^2}\right)} \mathcal{F}\left(u\left(x,z\right)\right)\right] \tag{II.20}$$

where $\mathcal{F}$ and $\mathcal{F}^{-1}$ are the forward and inverse Fourier transforms in (z,p) space. The small angle approximation, $\left|\frac{1}{k^2}\frac{\partial^2}{\partial z^2}\right| \ll 1$, indicates that $\frac{p^2}{k^2} = \sin^2\theta \ll 1$. FSS solution of standard PWE is obtained from the approximation to Q

$$Q \cong 1 + \frac{1}{2k^2}\frac{\partial^2}{\partial z^2} + \frac{(n^2(x,z)-1)}{2} \tag{II.21}$$

which is a suitable approximation for both small refractive index variations and small propagation angles. The approximation to Q stated in Eqn.II.19 has no restriction on propagation angles. Therefore, the FSS solution of WAPWE gives accurate results at angles up to nearly $\pm 45°$ [11, 12]. WAPWE is used to include large angles when modelling propagation over terrain.

II.6 Mixed Fourier Solution of the WAPWE

Kuttler and Dockery [5] developed the mixed Fourier transform for the PWE split step solution. The mixed Fourier transform (MFT) has permitted the extension of the Fourier split step method from propagation over smooth perfectly conducting surfaces to surfaces satisfying impedance boundary conditions. The mixed Fourier transform is defined as

$$U\left(x,p\right) = \int_0^\infty u\left(x,z\right)\left[\alpha\sin\left(pz\right) - p\cos\left(pz\right)\right]dz \tag{II.22}$$

and the inverse of this transform is given by

$$u\left(x,z\right) = \frac{2}{\pi}\int_0^\infty U\left(x,p\right)\left[\frac{\alpha\sin\left(pz\right) - p\cos\left(pz\right)}{\alpha^2+p^2}\right]dp + K\left(x\right)e^{-\alpha z} \tag{II.23}$$

where $K(x)$ is given by

$$K(x) = \begin{cases} 2\alpha \int_0^\infty u(x,z)\, e^{-\alpha z} dz & , \mathrm{Re}(\alpha) > 0 \\ 0 & , \mathrm{Re}(\alpha) \leq 0 \end{cases} . \tag{II.24}$$

Generally $\mathrm{Re}(\alpha) > 0$ for vertical polarization and $\mathrm{Re}(\alpha) < 0$ for horizontal polarization. Then the mixed Fourier split-step solution of Eqn.II.4 is

$$\begin{aligned} u(x+\triangle x, z) &= e^{\frac{jk\triangle x m(x,z)}{2}} \Big\{ e^{\frac{j\alpha^2 \triangle x}{2k}} e^{-\alpha z} K(x) \\ &+ \frac{2}{\pi} \int_0^\infty \left[\frac{\alpha \sin(pz) - p\cos(pz)}{\alpha^2 + p^2} \right] e^{\frac{-jp^2 \triangle x}{2k}} \\ &\times \left\{ \int_0^\infty u\left(x, z'\right) \left[\alpha \sin\left(pz'\right) - p\cos\left(pz'\right)\right] dz' \right\} dp \Big\} \end{aligned} \tag{II.25}$$

However, Eqn.II.25 requires two sine and two cosine transforms resulting in twice the time required for the Neumann or Dirichlet case. The discrete MFT split-step algorithm (DMFT) is used to implement this continuous MFT split-step algorithm based on expressions derived entirely in the discrete domain.

II.7 Boundary Conditions

II.7.1 The Upper Boundary Condition

In order to implement Eqn.II.7 using an FFT algorithm, an artificial upper boundary is established. To prevent strong reflections from the nonphysical upper boundary, the PWE solution field strength is smoothly attenuated or "filtered" above $z_{\max}$ to ensure that the field strength just below this boundary is reduced to zero. A cosine-taper (Hanning) window is applied to the upper quarter of the calculation height domain.

$$\text{Hanning Window} = 0.5 - 0.5\cos\left(i\frac{4\pi}{N_{\text{fft}}}\right), \text{ for } i = 0, 1, 2, ..., \frac{N_{\text{fft}}}{4}. \tag{II.26}$$

II.7.2 The Surface Boundary Condition

For the case of perfectly conducting flat surface Dirichlet and Neumann boundary conditions are applied for horizontal and vertical polarizations, respectively. To satisfy surface boundary conditions for non-perfectly conducting surface Leontovich boundary condition is used.

II.7.2.1 Dirichlet Boundary Condition

The boundary conditions state that the tangential fields must be continuous at the air/ground interface. In order to satisfy the boundary condition on a perfectly conducting surface, the tangential component of the electric field must vanish:

$$\overrightarrow{n} \times \overrightarrow{E} = 0 \tag{II.27}$$

where $\overrightarrow{n} = \overrightarrow{z}$ for flat surfaces. The reflection constant for horizontal polarization, R_H, over perfectly conducting ground is close to -1 ($|Z_s| \rightarrow \infty$) for plane waves incident at low grazing angle (even up to 10°), resulting in the Dirichlet's boundary condition, [11] :

$$u\left(x, 0\right) = 0. \tag{II.28}$$

The reflection coefficient is close to -1 for all frequencies above 100 MHz for almost all types of land for horizontal polarization. From image theory, a negative image is used for horizontal polarization to satisfy the boundary condition with odd u, i.e.

$$u\left(x, -z\right) = -u\left(x, z\right). \tag{II.29}$$

The sine transform enforces a Dirichlet boundary condition, which is equivalent to having a negative image source below the boundary or, in upper half-space, odd reflections from the boundary.

II.7.2.2 Neumann Boundary Condition

The normalized surface impedance for vertical polarization over perfectly conducting ground is close to 0 ($|Z_s| \rightarrow 0$) for plane waves incident at low grazing angle, resulting in the Neumann's boundary condition, [11] :

$$\frac{\partial u\left(x, 0\right)}{\partial z} = 0. \tag{II.30}$$

From image theory, a positive image is used for vertical polarization to satisfy the boundary condition with even u, i.e.

$$u\left(x, -z\right) = u\left(x, z\right). \tag{II.31}$$

The cosine transform enforces a Dirichlet boundary condition, which is equivalent to having a positive image source below the boundary or, in upper half-space, even reflections from boundary. The sum of the sine and cosine transform is equivalent to no image source and no reflections as if no boundary is present.

II.7.2.3 Leontovich Boundary Condition

Impedance boundary conditions are used to account for imperfectly conducting surfaces in propagation and scattering problems. To satisfy surface boundary conditions for finitely conducting earth, one can apply the Leontovich boundary condition:

$$\left.\frac{\partial u\left(x,0\right)}{\partial z}\right|_{z=0}+\alpha_{h,v}u\left(x,0\right)=0 \tag{II.32}$$

where α is defined as

$$\alpha=jk\sin\psi\left(\frac{1-R\left(x\right)}{1+R\left(x\right)}\right) \tag{II.33}$$

in which ψ is the grazing angle, and R is the polarization dependent Fresnel reflection coefficient, [6, 13, 5].

II.7.3 Reflection Coefficient

The polarization dependent Fresnel reflection coefficient, $R\left(x\right)$ is a function of surface impedance $Z_s\left(x\right)$, [14]. $R\left(x\right)$ is given as

$$R\left(x\right)=\frac{\sin\psi-Z_s\left(x\right)}{\sin\psi+Z_s\left(x\right)} \tag{II.34}$$

where

$$\begin{aligned} Z_s\left(x\right) &= \sqrt{n_c^2-\cos^2\psi}\text{ for horizontal polarization} \\ Z_s\left(x\right) &= \frac{\sqrt{n_c^2-\cos^2\psi}}{n_c^2}\text{ for vertical polarization.} \end{aligned} \tag{II.35}$$

When Eqn.II.35 is substituted into Eqn.II.34, we obtain

$$\begin{aligned} R_H\left(x\right) &= \frac{\sin\psi-\sqrt{n_c^2-\cos^2\psi}}{\sin\psi+\sqrt{n_c^2-\cos^2\psi}}\text{ for horizontal polarization} \\ R_V\left(x\right) &= \frac{n_c^2\sin\psi-\sqrt{n_c^2-\cos^2\psi}}{n_c^2\sin\psi+\sqrt{n_c^2-\cos^2\psi}}\text{ for vertical polarization} \end{aligned} \tag{II.36}$$

where the complex refractive index, n_c is defined as

$$n_c = \sqrt{\epsilon_r + j60\sigma\lambda}. \tag{II.37}$$

Here, the complex refractive index, n_c, is a function of the relative permittivity, ϵ_r, the conductivity, σ (S/m), and the wavelength λ, [7]. The relative permittivity ϵ_r and the conductivity σ (S/m) of different surface media are given in Table II.1.

Table II.1: Surface Medium Characteristics

Media Type	$\boldsymbol{\epsilon_r}$	$\boldsymbol{\sigma}$ (mS/m)
Air	1	0
Ice	3-4	0.01
Fresh Water	80	0.5
Salt Water	80	3000
Dry Sand	3-5	0.01
Wet Sand	20-30	0.01-1
Shales and clays	5-20	1-1000
Silts	5-30	1-100
Limestone	4-8	0.5-2.0
Granite	4-6	0.01-1
(dry) salt	5-6	0.01-1
Poor Gound	4	1
Average Ground	15	5
Good Ground	25	20
Fresh Water	81	10
Sea Water	81	5000
Icy Ground	3.2	5
Dry Ground	5	1
Soil	10	10
Forest	10	20
Land	15	1
Wet Ground	15	50

When Eqn.II.36 is substituted into Eqn.II.33, we obtain

$$\begin{aligned} \alpha_h &= jk\sqrt{n_c^2 - \cos^2\psi} \text{ for horizontal polarization} \\ \alpha_v &= \frac{jk\sqrt{n_c^2 - \cos^2\psi}}{n_c^2} \text{ for vertical polarization.} \end{aligned} \tag{II.38}$$

For low grazing angles, $\cos^2\psi \cong 1$

$$\begin{aligned} \alpha_h &\cong jk\sqrt{n_c^2 - 1} \text{ for horizontal polarization} \\ \alpha_v &\cong \frac{jk\sqrt{n_c^2 - 1}}{n_c^2} \text{ for vertical polarization.} \end{aligned} \tag{II.39}$$

After making an additional approximation $|n_c^2| \gg 1$, we can derive

$$\begin{aligned} \alpha_h &\cong jkn_c \text{ for horizontal polarization} \\ \alpha_v &\cong \frac{jk}{n_c} \text{ for vertical polarization.} \end{aligned} \tag{II.40}$$

These Leontovich Coefficients (II.39,II.40) are independent of the grazing angle ψ. The smooth surface Fresnel reflection coefficient, $R(x)$, can be modified to model surface roughness [6] as follows

$$R_{\text{eff}}(x) = \rho R(x) \tag{II.41}$$

where ρ is the roughness reduction factor.

II.8 Irregular Terrain Modelling

II.8.1 Staircase Terrain Modelling

This approach assumes that the ground does not support propagation at the wavelength of interest and the terrain is modelled with successive horizontal segments. Terrain effects at each range step are included by setting the array elements below the level of the terrain to zero, [15]. This is equivalent to representing the boundary by a series of knife-edge diffractors, [13], and neglecting backscatter due to corner diffraction. This method simply inserts a perfectly conducting knife-edge at each range with height equivalent to the terrain height at that range. When stair case terrain modelling is used, the boundary conditions on sloping facets are not properly accounted for.

II.8.2 Conformal Mapping

The Fourier split-step solution of the parabolic wave equation requires a flat surface. Thus, a coordinate transformation is made by

$$\begin{aligned} \chi &= x \\ \zeta &= z - T(\chi) \end{aligned} \tag{II.42}$$

where the function $T(\chi)$ describes the actual terrain. The scalar component of the field in terms of the new coordinate system is given by

$$v\left(\chi,\zeta\right)=u\left(x,z\right)e^{-j\left[k\zeta\frac{\partial T}{\partial\chi}+\frac{k}{2}\int_{0}^{\chi}\left(\frac{\partial T}{\partial s}\right)^{2}ds\right]} \tag{II.43}$$

Then, the Fourier split-step solution of the terrain parabolic wave equation becomes

$$v\left(\chi+\triangle\chi,\zeta\right)=e^{\frac{jk\triangle\chi\left(n^{2}(\zeta+T(\chi))-1-2\zeta\frac{\partial^{2}T}{\partial\chi^{2}}\right)}{2}}\mathcal{F}^{-1}\left[e^{\frac{-j\triangle\chi p^{2}}{2k}}\mathcal{F}\left(v\left(\chi,\zeta\right)\right)\right] \tag{II.44}$$

where the terrain effects are taken into account by the second derivative of the terrain with respect to range, [7, 14, 4].

A simpler boundary condition is obtained by making the coordinate transformation. The boundary condition, $v\left(\chi,T(\chi)\right)=0$, is satisfied by odd symmetry of the field given by, [19]

$$v\left(\chi,-\zeta+2T(\chi)\right)=-v\left(\chi,\zeta\right) \tag{II.45}$$

CHAPTER III

SIMULATION RESULTS

III.1 General Description

The parabolic approximation of Helmholtz equation can be done using different techniques. The narrow angle and wide angle approaches are the two main formalisms of the PWE method. Various boundary mapping methods together with different boundary conditions are used in the models. Radar Propagation Prediction Tool (RPPT) is a MATLAB computer program which uses the Parabolic Equation method for radio wave propagation in the atmosphere. There exists four models in the RPPT Software written in MATLAB (Version 6.0). These models, which use different solutions to PWE, are ;

Model 1: SPWE (Staircase Terrain Modelling)

Model 2: SPWE (Conformal Terrain Modelling)

Model 3: SPWE (Staircase Terrain Modelling & Sine Transform)

Model 4: WAPWE (Staircase Terrain Modelling)

RPPT uses four functions; Spe_Staircase, Spe_Conformal, Spe_SinCos and WAPWE. Each of these functions form a different propagation model.

The user interface comprises of two windows; main window and parameter setting window. RPPT Main Window (Fig.III.1) enables to select the propagation model. Propagation Model Settings Window (Fig.III.2) enables to change the parameters used in the model. Some of the edit boxes are disabled due to a

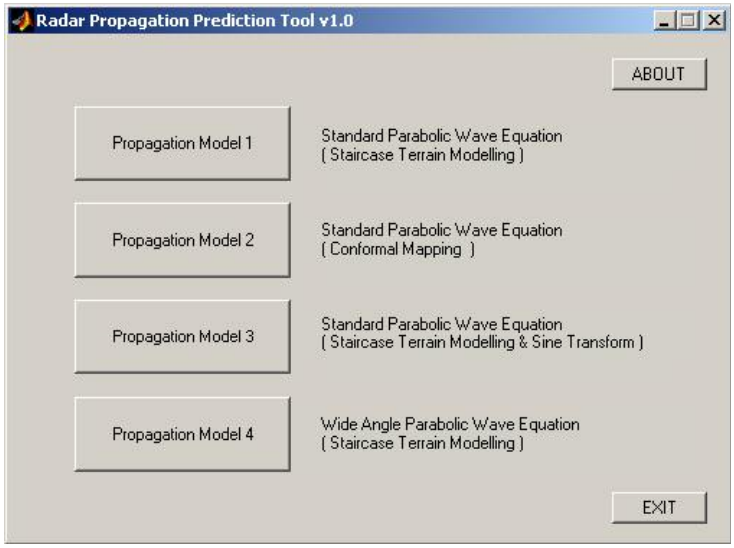

Figure III.1: Radar Propagation Prediction Tool (RPPT) Main Window.

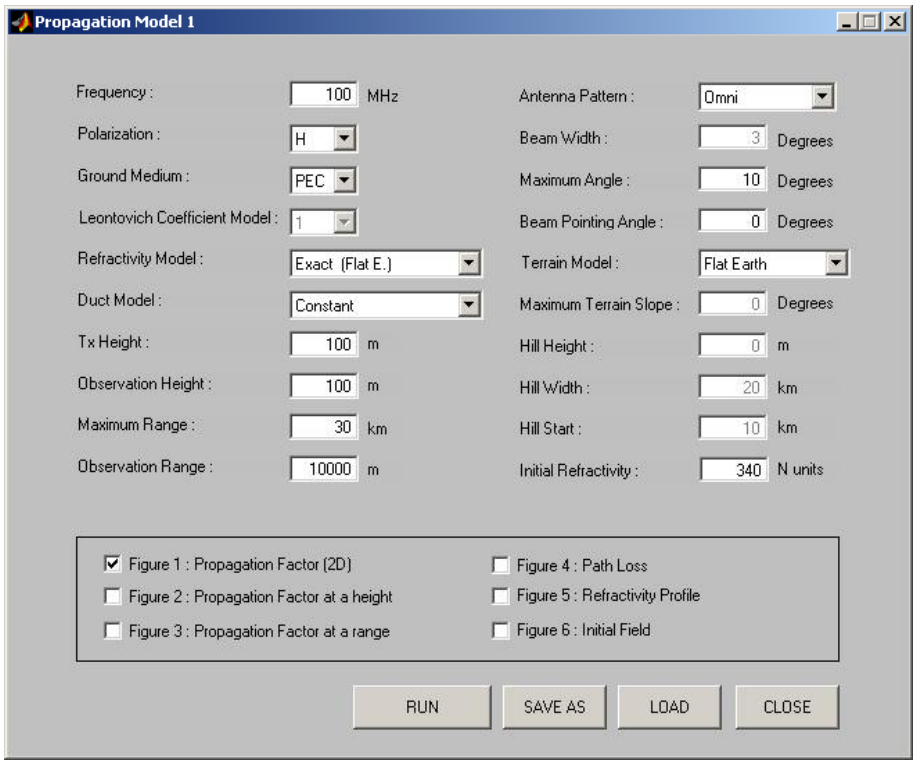

Figure III.2: Propagation Model Settings Window.

selection of a related combo box option. 'Leontovich Coefficient Model' is related to 'Ground Medium'. When 'Leontovich Coefficient Model' is set to '1', grazing angle is taken into account in the calculations (Eqn.II.38). However, when it is set to '2', zero grazing angle is assumed (Eqn.II.39), and when it is set to '3' zero grazing angle with the complex refractive index, n_c, much bigger than 1 is assumed, and when it is set to '4' (Eqn.II.40), α, is calculated using Fresnel reflection coefficient, $R(x)$, which assumes non-zero grazing angle as stated in Eqn.II.33. 'Beam Width' is related with 'Antenna Pattern'. 'Maximum Terrain Slope', 'Hill Height', 'Hill Width' and 'Hill Start' are related to 'Terrain Model'. The user is allowed to select the type of the graph among six options. The selection of the graph type does not change the execution time. It is possible to edit the source code of the functions and by following the comments, one could change further parameters.

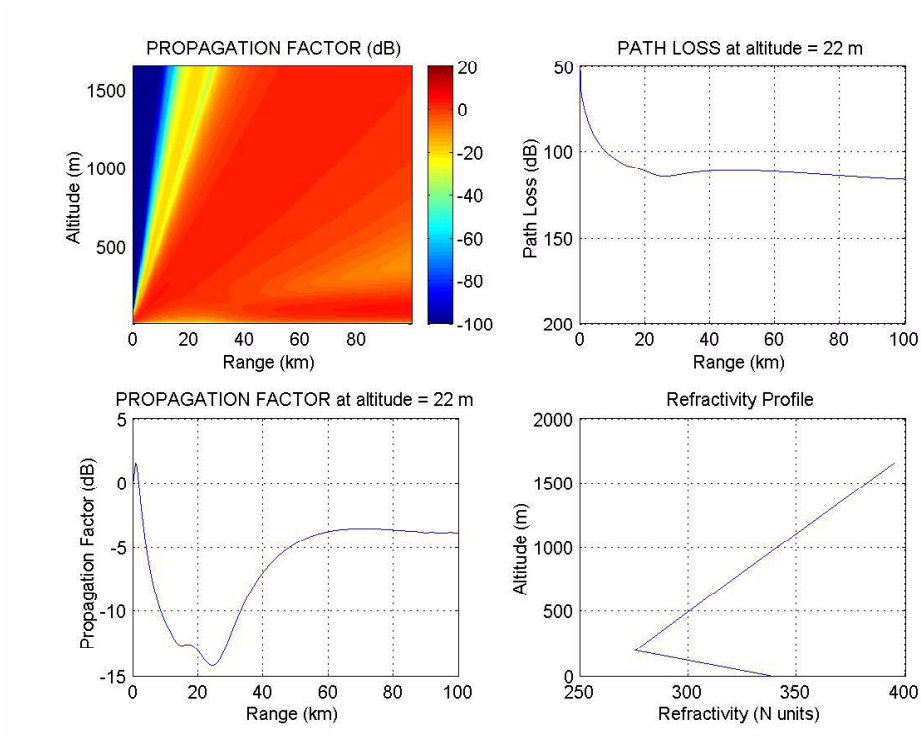

Figure III.3: Surface Based Duct with SPWE.
Two linear segments are used with a trapping layer height of 200 m.
(f = 100 MHz, H-pol, Flat Earth, PEC Surface, Gaussian Antenna Pattern,
Tx Height = 22 m, Observation Height = 22 m).

It is possible to save and load settings for RPPT models. While saving the settings both an m -file and a text file are formed. While loading the settings, m - file is used. Text file is used for documentation purposes and to call the function from Matlab command window.

RPPT can plot 6 selectable diagrams: Propagation Factor (2D), Propagation Factor at a height, Propagation Factor at a range, Path Loss, Refractivity Profile and Initial Field. Refractivity profiles of Constant, Linear, Surface Layer and Elevated Layer are available (Fig.III.3). The refractivity profile is stored in an $M \times N$ matrix where M, N are the number of range and vertical increments, respectively. Thus, it is possible to assess range dependent refractivity profiles with modifying the code. Program offers omni and gaussian antenna patterns (See Appendix C). Propagation Factor and Path Loss are shown in dB's.

III.2 Results Of Different Approaches

RPPT can calculate electromagnetic propagation over terrain at low grazing angles. The physical domain with an irregular boundary is mapped to a rectangular domain. By neglecting backscattered wave energy and restricting propagation to small angles with respect to the horizon, accurate results are obtained over tens or even hundreds of kilometers in range. The effects of atmospheric refraction are also taken into account by modifying the refractive index $n(x, z)$. RPPT can easily assess the effects of different duct models (See Appendix E).

The results are discussed and compared with other propagation modelling softwares, CARPET and RADCAL. Both of these programs use ray optics method for modelling. The relevant settings of the figures shown in the whole document are saved in appropriately named files for RPPT, CARPET and RADCAL. To demonstrate the comparisons, propagation factor and path loss are mainly used. (See Appendix A). Propagation factor and path loss are expressed in dB's (y-axis), and range is expressed in km's (x-axis).

A comparison with the analytic data is made for a horizontally polarized wave propagating above a perfectly conducting surface. Analytic plot is obtained by summing the two separate ray paths. One is the direct path from the transmitter;

the other is the path reflected from the surface of the earth. The total phase difference between the direct and the ground reflected signal is calculated at the observation height.

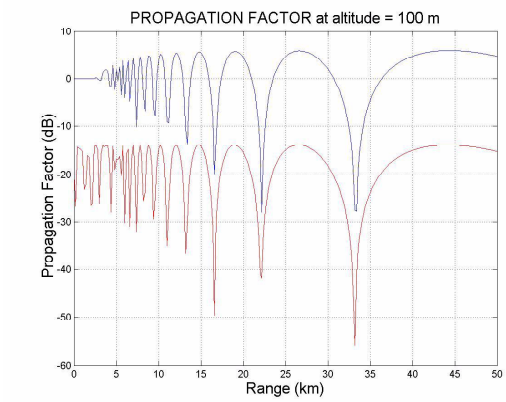

Figure III.4: SPWE and Analytic data.
(f = 1 GHz, H-pol, Flat Earth, PEC Surface, Gaussian Antenna Pattern,
Tx Height = 100 m, Observation Height = 100 m)

The analytic data is shown with a -20 dB offset to separate the two graphs. It is quite clear that the results are similar after 5 km of range.

III.2.1 Variation of FFT size and time (100MHz, 1GHz, 3GHz)

The execution time of RPPT which is critical for the selection of frequency and range, is assessed by running the program in a computer.

Table III.1: FFT Size and Time for SPWE.

	SPWE		**WAPWE**	
Frequency	**FFT Size (MxN)**	**Time (Sec.)**	**FFT Size (MxN)**	**Time (Sec.)**
100MHz	97 x 256	1.87	172 x 512	104.71
1GHz	172 x 2048	15.45	172 x 2048	2001.6
3GHz	172 x 4096	37.81	172 x 2048	2010.3

The split-step PE method requires extensive memory and computation (See Appendix B). A larger maximum angle, higher frequency and longer range lead to a larger transform size and a longer execution time as seen from Table III.1. The computational time of the algorithm is proportional to $M \times N \log_2(N)$ where M, N are the number of range and vertical increments, respectively, [11]. The

computations are done on a 2.40 GHz Intel Pentium 4 PC with 256 MB RAM. The results shown at Table III.1 are obtained by running RPPT Model1 and Model2 several times at 30km of range. During the computations, maximum propagation angle is assumed 10° for SPWE and 30° for WAPWE. There are some limitations for the maximum range step size and FFT number in the Matlab code for avoiding memory errors.

III.2.2 Variation of Maximum Propagation Angle with SPWE and WAPWE

SPWE gives accurate results for angles up to nearly 15° while, WAPWE gives accurate results for angles up to nearly 45°. For SPWE, maximum propagation angle $\theta_{\max}$ is determined as

$$\begin{aligned} \theta_{\max} &= 10^\circ \text{ for } f > 1000 \text{ MHz} \\ \theta_{\max} &= 15^\circ \text{ for } f \leq 1000 \text{ MHz.} \end{aligned} \tag{III.1}$$

The solution of SPWE clearly breaks down above 25°. The causes of this problem are commutator error, split-step solution error and approximate expansion of the operator square root, [13].

WAPWE gives good results in the deep shadow regions. If the angle exceeds 50° in WAPWE, one should use very small vertical and range increments to avoid aliasing effects and the method consequently loses its computational advantage. SPWE is applicable at frequencies from 100 MHz through the microwave range. The lower frequency limit is set by the onset of surface wave and the upper frequency is limited by propagation mechanism not accounted during present methodology such as the effect of precipitation.

III.2.3 Horizontal versus Vertical Polarization with WAPWE

RPPT outputs of horizontally and vertically polarized wave propagation in the troposphere are compared.

The main difference between horizontally and vertically polarized waves is the boundary conditions that are enforced at the Earth's surface. For a standard

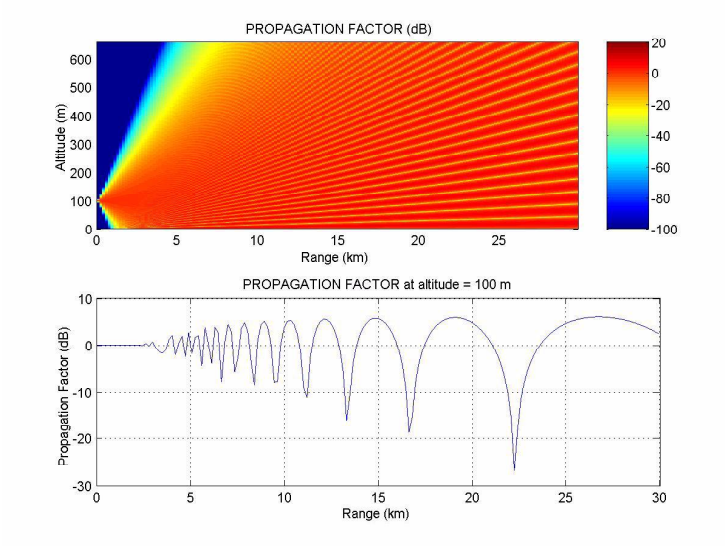

Figure III.5: Horizontally Polarized Wave Propagation.
(f = 1 GHz, H-pol, Flat Earth, PEC Surface, Gaussian Antenna Pattern,
Tx Height = 100 m, Observation Height = 100 m)

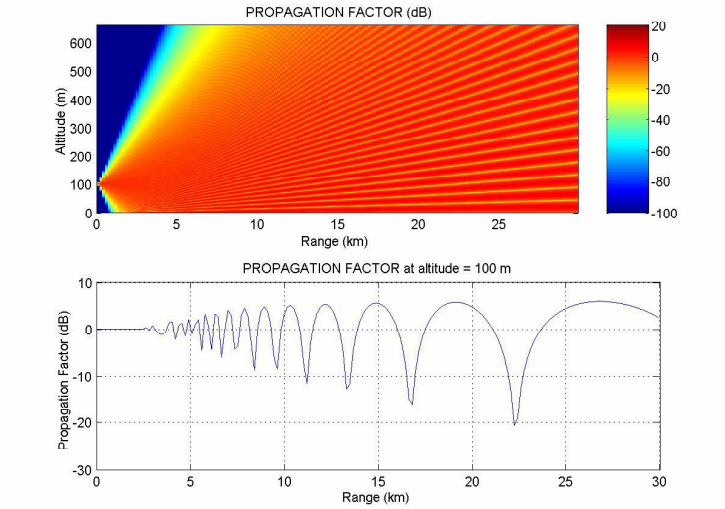

Figure III.6: Vertically Polarized Wave Propagation.
(f = 1 GHz, V-pol, Flat Earth, PEC Surface, Gaussian Antenna Pattern,
Tx Height = 100 m, Observation Height = 100 m)

atmosphere and smooth sea, the primary effect of polarization is seen in the null depths and peak heights in the interference region as in Fig.III.5 and Fig.III.6; vertically polarized fields have a reflected amplitude that is smaller than that for horizontal polarization, which causes less severe nulls over the same range of angles, [16]. The polarization differences are expected to be more significant for weakly conducting surfaces such as dry ground at lower frequencies. There is significant penetration of the fields into the geometrical shadow zones, particularly for vertically polarized waves, [17]. Other polarizations can be obtained from a linear combination of vertically and horizontally polarized fields, [5].

III.2.4 Flat Earth and Flattened Earth Models with SPWE

RPPT outputs of flat earth and flattened earth are compared with respect to range and height.

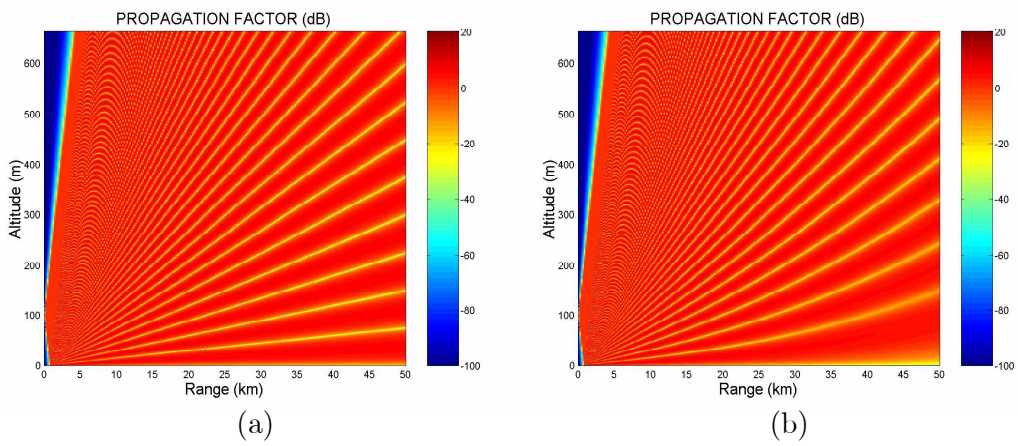

(a) (b)

Figure III.7: Flat Earth (a) and Flattened Earth (b) Models.
(f = 1 GHz, H-pol, PEC Surface, Omni Antenna Pattern,
Tx Height = 100 m, Observation Height = 100 m)

As a result of the earth flattening, the waves bend upwards in Fig.III.7b compared to Fig.III.7a. However, at short ranges, the outputs of both models are similar. While making earth flattening transformation, effective earth radius is used. The results show good agreement between other propagation programs.

The modified index of refraction, $m(x, z)$, which accounts for earth's curvature is valid for low altitudes ($h \leq 5$ km) and short ranges ($x \leq 500$ km). The term $\frac{2z}{a}$

accounts for the spherical shape of earth, when it is neglected, the refractive index, $n(x, z)$, describes propagation over flat earth. The approximate $m(x, z)$ is valid for lower altitudes where $\left(\frac{z}{a}\right)^2 \ll 1$. The logarithmic height transformation should be used to model higher altitudes because the usual flat earth approximation loses accuracy at larger heights (See Appendix E.4).

III.2.5 Staircase versus Conformal Mapping with SPWE (Rectangle, Pyramid, Sinuson, Sinusoidal)

RPPT can handle various irregular terrain profiles. The geometry of the terrain is stored in an array of size 1xM where M is the number of range increments. RPPT offers some predefined terrain geometries (See Appendix D). However, the importation of the terrain profile from a standard digital dataset (Digital Terrain Elevation Data (DTED)) can be easily implemented. DTED is a uniform matrix of terrain elevation values which provides basic quantitative data for systems and applications that require terrain elevation, slope, and/or surface roughness information. To make the profile suitable for propagation predictions, a smoothing algorithm should be applied.

The surface reflections and the degree of shadowing behind the obstacles are compared for staircase and conformal mapping. The results are obtained at perfectly conducting surfaces with 1 GHz frequency and horizontal polarization.

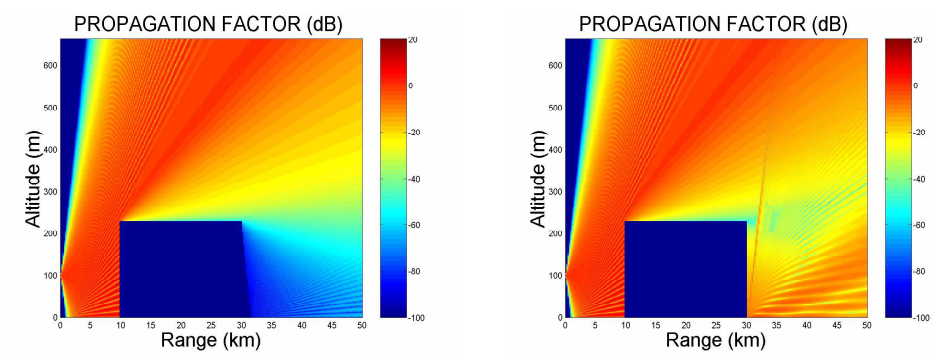

(a) (b)

Figure III.8: Rectangle Hill with Staircase (a) versus Conformal (b) Mapping. (f = 1 GHz, H-pol, PEC Surface, Gaussian Antenna Pattern, Tx Height = 100 m, Observation Height = 100 m, Hill Height = 229 m).

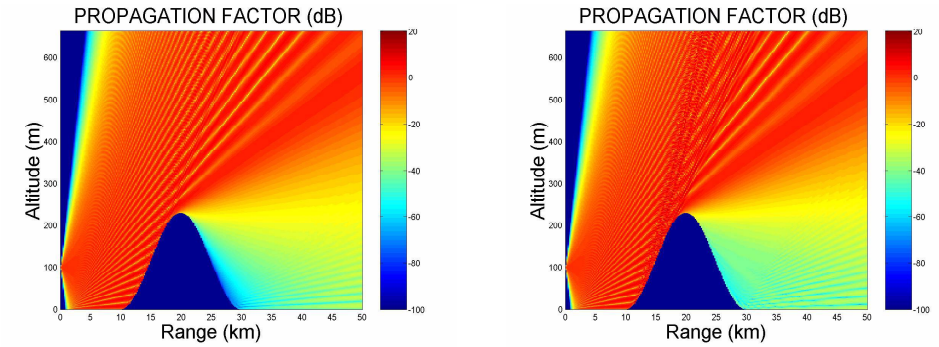

(a) (b)

Figure III.9: Sinuson Hill with Staircase (a) versus Conformal (b) Mapping. (f = 1 GHz, H-pol, Flat Earth, PEC Surface, Gaussian Antenna Pattern, Tx Height = 100 m, Observation Height = 100 m, Hill Height = 229 m).

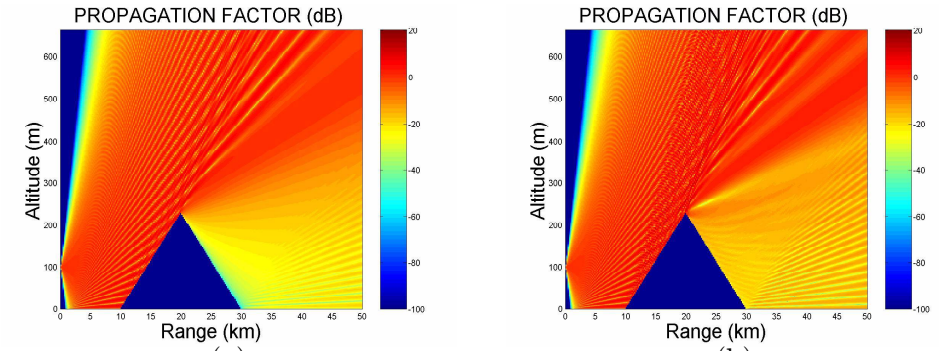

(a) (b)

Figure III.10: Pyramid Hill with Staircase (a) versus Conformal (b) Mapping. (f = 1 GHz, H-pol, Flat Earth, PEC Surface, Gaussian Antenna Pattern, Tx Height = 100 m, Observation Height = 100 m, Hill Height = 229 m).

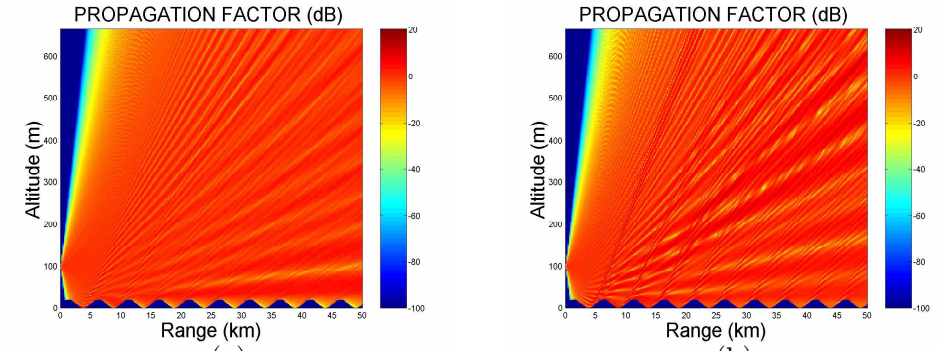

(a) (b)

Figure III.11: Sinusoidal Hill with Staircase (a) versus Conformal (b) Mapping. (f = 1 GHz, H-pol, Flat Earth, PEC Surface, Gaussian Antenna Pattern, Tx Height = 100 m, Observation Height = 100 m, Hill Height = 20 m).

The main difference between Fig.III.10 and Fig.III.9 is the attenuation in the shadowing beyond the peak of the obstacle. The strong diffraction of the incident field by the vertex of the pyramid, resulted in significantly increased field strength well into the geometric shadow zone.

Strong reflections from the front faces of sinuson hill (Fig.III.9.b) and pyramid hill (Fig.III.10.b) are seen in figures formed by conformal mapping. However, there exists weak reflections in figures formed by staircase mapping. Thus, conformal mapping can predict deeper shadow regions behind each of the obstacle. There is weak shadowing of the incident field beyond the peak which is very nearly geometric. The significant difference between Figs. III.9.b and III.10.b is the contrast in the shadowing beyond the peak of the obstacles. There is strong diffraction by the vertex of the pyramid which is important in radar-terrain applications.

In staircase mapping the surface reflections are lost by approximating the surface by a series of knife-edge diffractors as seen in Fig.III.11. As a result, staircase mapping is a poor approximation.

In Figs. III.8.b, III.9.b and III.10.b a very slight distortion of the field is observed near the vertices due to the discontinuous change in surface slope. Conformal mapping can handle discontinuous slope changes on the order of 15-20°, [13]. To accommodate a larger range of slopes, a hybrid of conformal mapping (shift map) with the well-known staircase mapping (terrain masking) approximation can be used, [13].

III.2.6 Ground Wave Propagation with WAPWE

Ground wave propagation is simulated above a sea-land-sea type ground medium with vertical polarization, gaussian antenna pattern and flat earth. While modelling sea, relative permittivity, ϵ_r, of 70 and conductivity, σ, of 5 S/m is used. Land is modelled by relative permittivity, ϵ_r, of 30 and conductivity, σ, of 0.01 S/m. The first boundary (sea-land) exists at 94,175 m's and the second boundary (land-sea) exists at 192,117 m's away from the radar.

The ground waves are formed by direct, reflected and surface waves. Surface

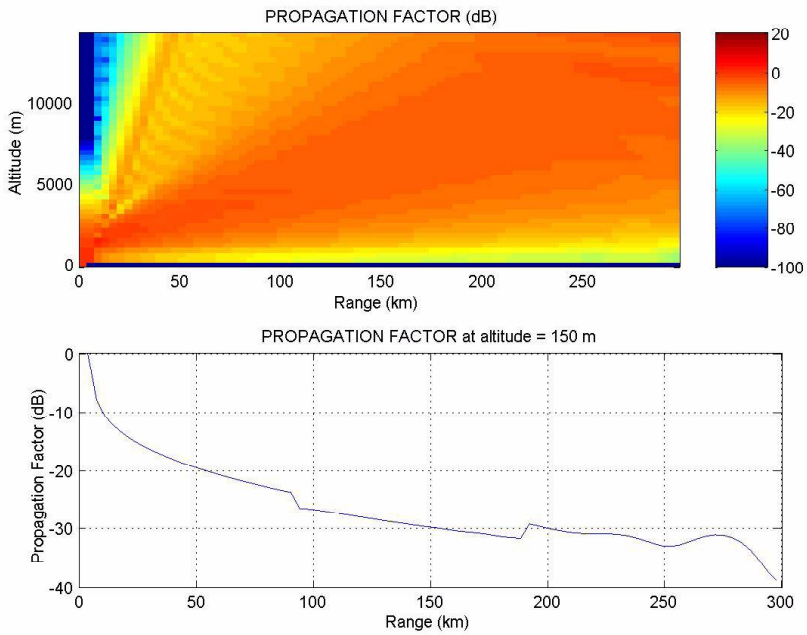

Figure III.12: Ground Wave Propagation with SPWE.
(f = 1 MHz, V-pol, Flat Earth, Sea-Land-Sea Surface,
Gaussian Antenna Pattern, Tx Height = 150 m, Observation Height = 150 m)

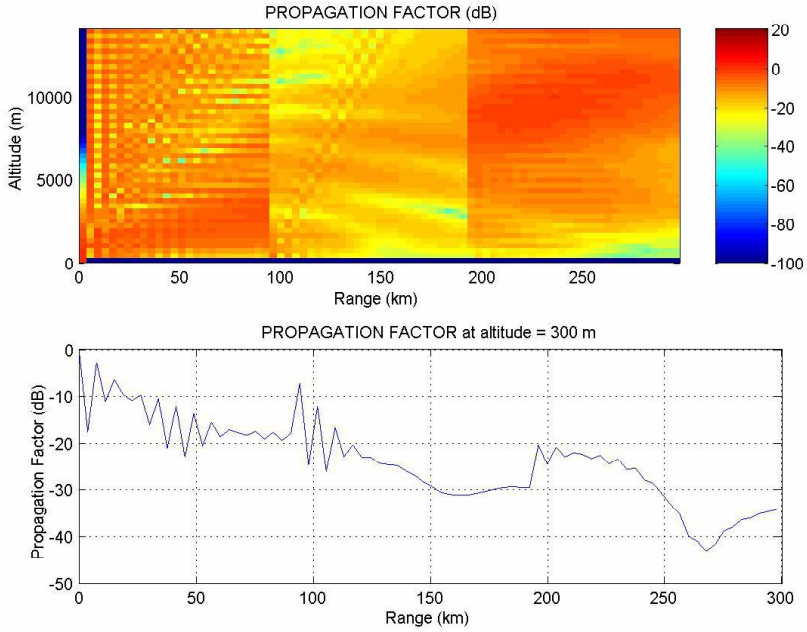

Figure III.13: Ground Wave Propagation with WAPWE.
(f = 1 MHz, V-pol, Flat Earth, Sea-Land-Sea Surface,
Gaussian Antenna Pattern, Tx Height = 300 m, Observation Height = 300 m).

waves propagate along the surface of the earth. While passing over the ground, surface wave induces a voltage. The induced voltage attenuates the wave. This attenuation depends on the electrical properties of the terrain, frequency and polarization. For vertical polarization or at lower frequencies, the electric field is attenuated less. At low frequencies (1 kHz to 3 MHz) the interface between air and the ground acts like an efficient waveguide for vertical polarization. The recovery effect which has been observed experimentally by Millington and Isted takes place due to multiple segments having different ground constants. The DMFT solution of WAPWE is used for correct modelling of reflection effects at vertical polarization and for the modelling of propagation over rough surfaces.

In Fig.III.12 and Fig.III.13, the ground medium comprises of sea-land-sea surfaces. However, RPPT could not manage to handle ground wave propagation accurately and the recovery effect is not clear at the land/sea boundary.

III.3 Comparison With CARPET

CARPET (Computer Aided Radar Performance Evaluation Tool) is a computer tool for the assessment and design of the surface-based radars. It is developed at the TNO Physics and Electronics Laboratory by Albert G. Huizing and Arne Theil. CARPET takes into account the entire radar system and its environment, including: transmitter/receiver characteristics, clutter, jamming, antenna, and propagation phenomena. RPPT models are compared with CARPET Software using the propagation factor diagrams.

As seen from Figs.III.14, III.15 and III.16 there is significant similarity between the outputs of CARPET and RPPT. However, there exists some differences in the amplitudes of null depths. The cause of this could be the differences in the variety of input parameters required by both programs. CARPET is run by the settings stated in Fig.III.17

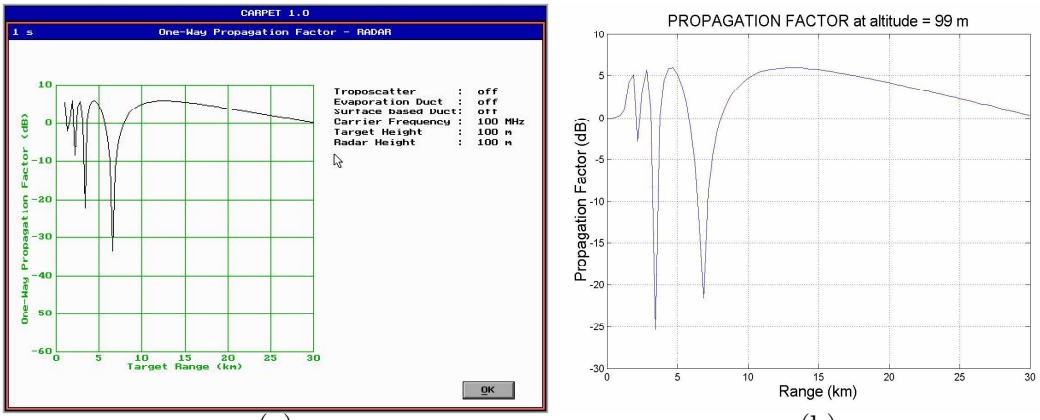

(a) (b)

Figure III.14: CARPET (a) vs RPPT (b) output at 100 Mhz.
(f = 100 MHz, H-pol, Flattened Earth, PEC Surface, Omni Antenna Pattern,
Tx Height = 100 m, Observation Height = 100 m)

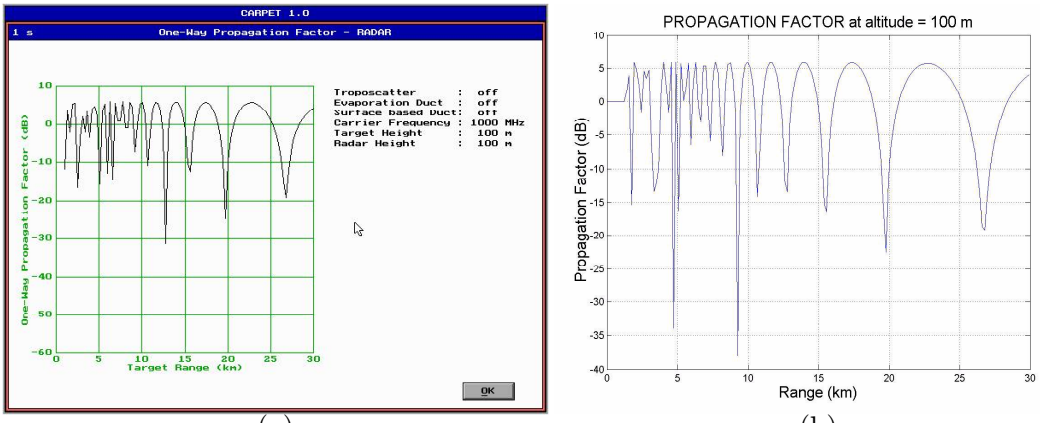

(a) (b)

Figure III.15: CARPET (a) vs RPPT (b) output at 1 GHz.
(f = 1 GHz, H-pol, Flattened Earth, PEC Surface, Omni Antenna Pattern,
Tx Height = 100 m, Observation Height = 100 m)

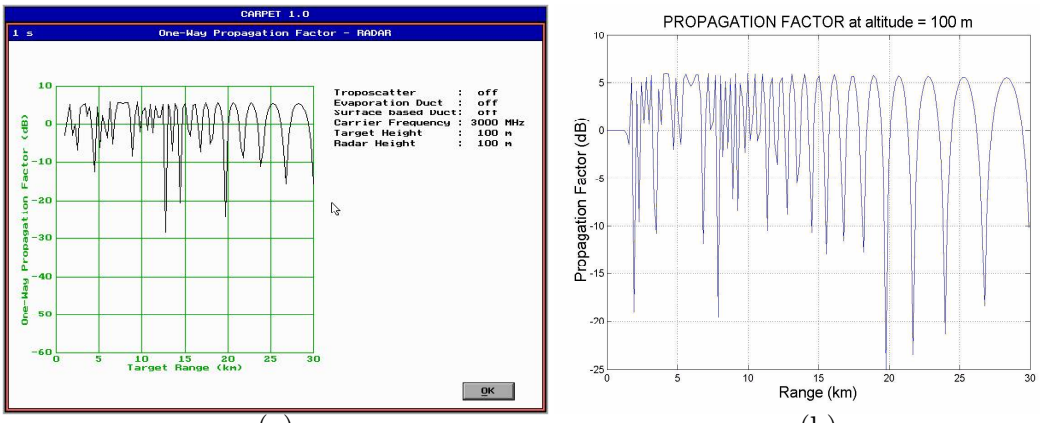

(a) (b)

Figure III.16: CARPET (a) vs RPPT (b) output at 3 GHz.
(f = 3 GHz, H-pol, Flattened Earth, PEC Surface, Omni Antenna Pattern, Tx Height = 100 m, Observation Height = 100 m)

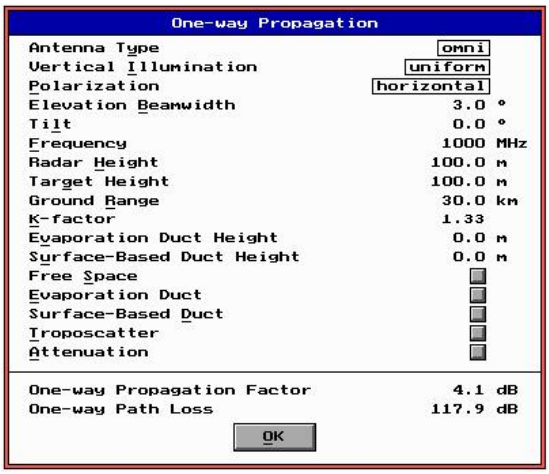

Figure III.17: CARPET Settings.

III.4 Comparison With RADCAL

RADCAL (Radar Calculation Program) was first developed by A.Hızal for radar simulation. Later, the new version of RADCAL is developed by O.Şengül in both Pascal and C++ programming languages, [20]. RADCAL considers radar, target, jammer, environment and terrain dependent parameters. It uses five-ray propagation model for reflection and diffraction. Terrain type, atmospheric diffraction and ground clutter have been included in the calculations. The output of RADCAL is the graph of the effective signal to noise+clutter ratio versus range. In order to make comparisons with RPPT, C++ version of RADCAL program is modified with the guidance of O.Şengül to plot the one-way propagation factor.

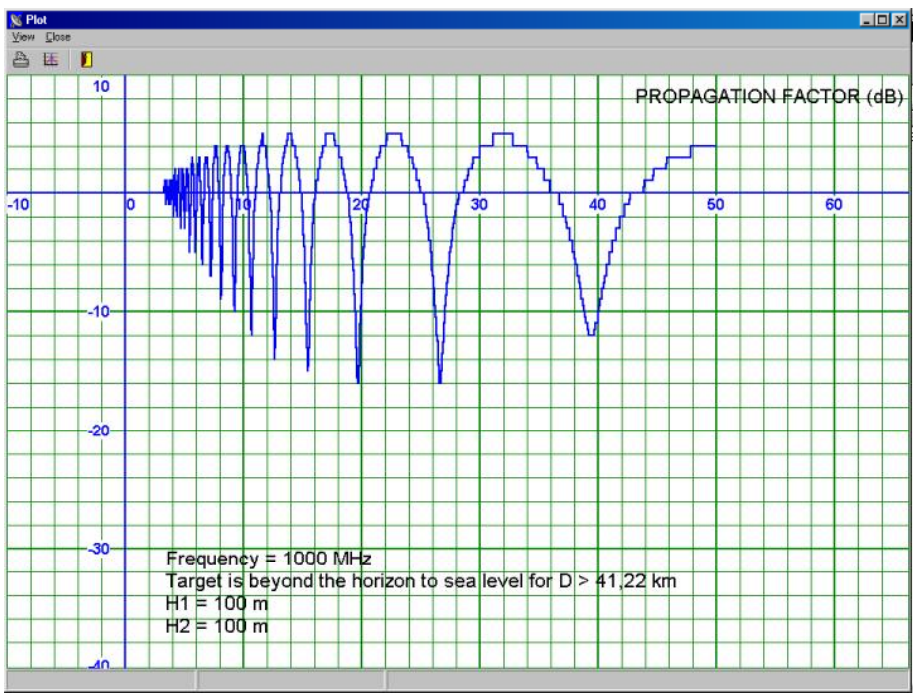

Figure III.18: RADCAL output at 1 GHz over flattened Earth.
(f = 1 GHz, H-pol, Flattened Earth, Land Surface, Beam Width = 3°,
Tx Height = 100 m, Observation Height = 100 m)

It can be seen from Fig.III.18 and Fig.III.19 that the outputs of RADCAL and RPPT show a very strong correlation. The plots are obtained considering flattened earth without any hills.

To assess the scattering effects of a hill between the radar and target, two scenarios are considered. During the execution of the scenarios, flattened earth

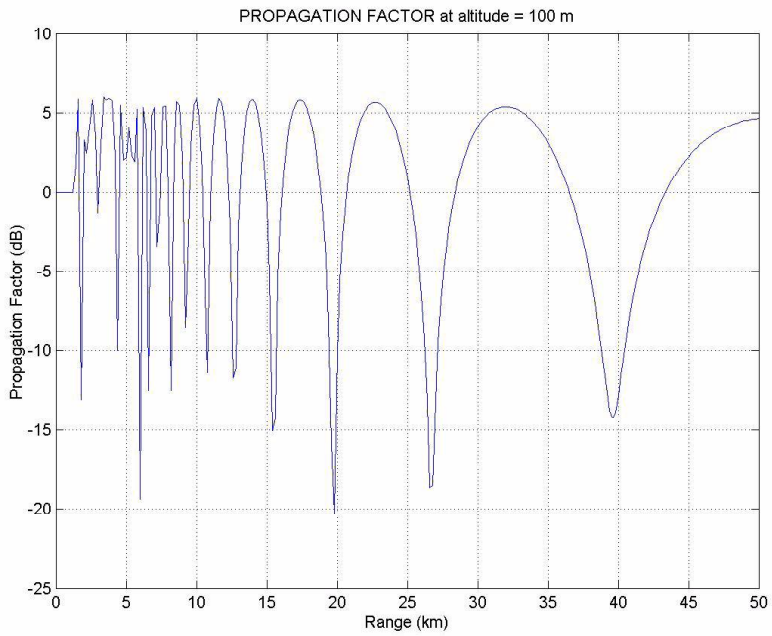

Figure III.19: RPPT output at 1 GHz over flattened Earth.
(f = 1 GHz, H-pol, Flattened Earth, PEC Surface, Omni Antenna Pattern,
Tx Height = 100 m, Observation Height = 100 m).

model with horizontal polarization at 1 GHz frequency is assumed. At first, the height of the hill (Fig.III.24.a) is below Radar/Target height where LOS (Line of Sight) propagation is dominant. The hill is 100 m high and placed at 25 km's away from the radar.

A slight distortion of the field is observed due to the reflections from the hill surface after 25 km's in Fig.III.21 obtained from RPPT Model2 which uses conformal mapping technique. However, the field distortion is observed after 40 km's in RADCAL as seen in Fig.III.20. It should be noted that the reflections from a hill surface strongly depend on the shape of the hill. Thus, the outputs of both programs are not expected to be exactly same because of the differences in the hill shape definitions.

At the second scenario, the height of the hill (Fig.III.24.b) is above Radar/Target height. The hill is 229 m high and placed at 25 km's away from the radar.

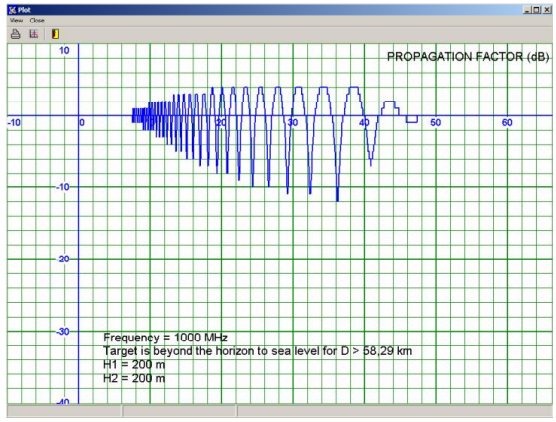

Figure III.20: RADCAL output over a hill below LOS.
(f = 1 GHz, H-pol, Flattened Earth, Land Surface, Beam Width = 3°,
Tx Height = 200 m, Observation Height = 200 m, Hill Height = 100 m)

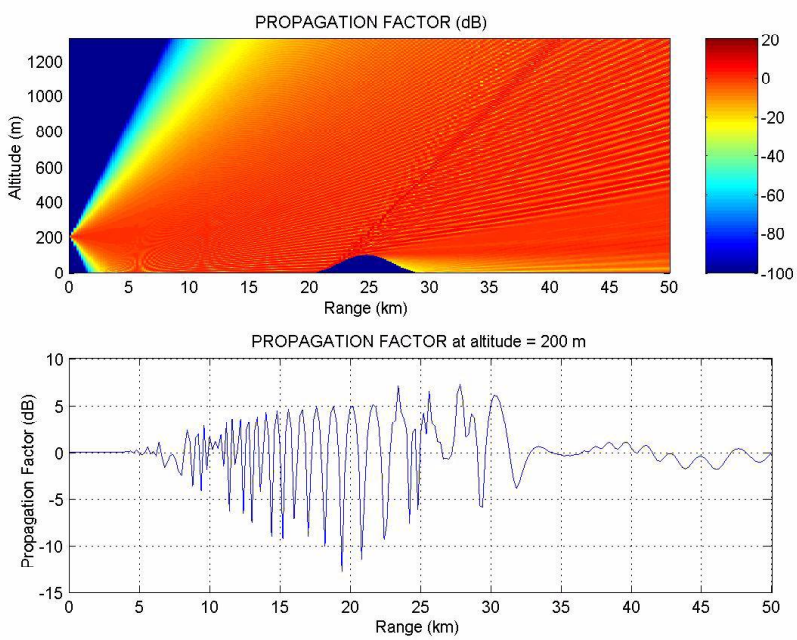

Figure III.21: RPPT output over a sinuson hill below LOS.
(f = 1 GHz, H-pol, Flattened Earth, PEC Surface, Gaussian Antenna Pattern,
Tx Height = 200 m, Observation Height = 200 m, Hill Height = 100 m).

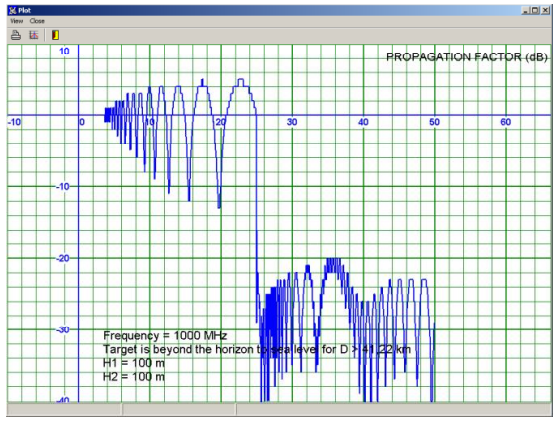

Figure III.22: RADCAL output over a hill obscuring LOS.
(f = 1 GHz, H-pol, Flattened Earth, Land Surface, Beam Width = 3°,
Tx Height = 100 m, Observation Height = 100 m, Hill Height = 229 m)

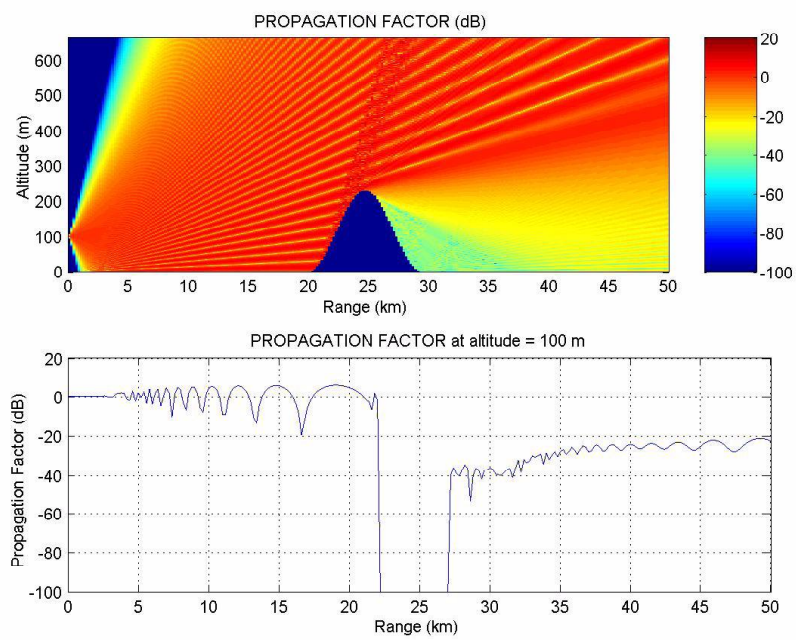

Figure III.23: RPPT output over a sinuson hill obscuring LOS.
(f = 1 GHz, H-pol, Flattened Earth, PEC Surface, Gaussian Antenna Pattern,
Tx Height = 100 m, Observation Height = 100 m, Hill Height = 229 m).

When the shadow regions are compared in Fig.III.22 and Fig.III.23, the difference is not quite clear. Both figures show non-zero field strength behind the obstacles due to diffraction from the hill top.

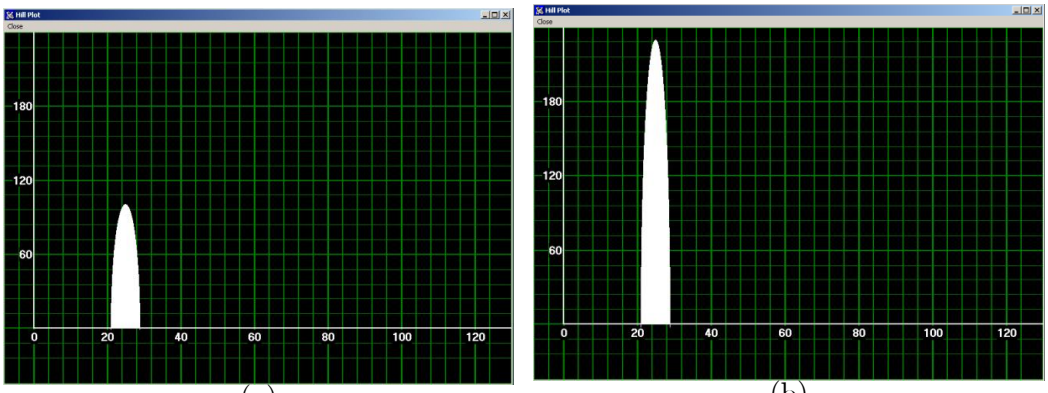

(a) (b)

Figure III.24: RADCAL Hills with 100 m (a) and 229 m (b) height.
(Horizontal axis represents range and vertical axis represents height.)

The execution time of RADCAL is much shorter than RPPT. However, a better comparison of the speed could be possible when RPPT is rewritten in C++.

CHAPTER IV

CONCLUSION AND FUTURE WORK

IV.1 Conclusion

The 2D problem of radio wave propagation over irregular terrain is solved by the parabolic equation approximation of the Helmholtz wave equation. PWE is solved by marching over range steps. An initial transverse field distribution, $u\left(x_0, z\right)$ is injected to PWE Model and is longitudinally propagated through a medium defined by its refractive index profile $n(x, z)$. FSS solution of the PWE is efficient and reliable for propagation modelling over weakly backscattering rough surfaces with varying refractivity profile. This model is based on the assumption that the propagation takes place at low grazing angles. A Hanning window is used to attenuate the field smoothly at large heights and large propagation angles to avoid reflections from nonphysical upper boundary. The challenging problem is to satisfy the surface boundary conditions for non-perfectly conducting surface using the impedance boundary conditions.

RPPT is developed for use in tropospheric radiowave propagation. It is based on the split-step Fourier solution of the PWE, which has been shown to be numerically efficient. Both horizontal and vertical polarizations are considered in the model. RPPT is a powerful tool to predict multipath and ducting. The narrow and wide angle propagators are also compared to quantify the improvement of SPWE over WAPWE. To validate RPPT, comparisons are made against other

propagation models such as CARPET and RADCAL.

PWE models are currently used in propagation simulations, radar coverage predictions, trade-off studies, design evaluations, analyses of experiments and at sea tests. Less experienced users should pay special attention while using PWE models, because they may fail in an unremarkable way which may go unnoticed. Such as, some negative values and steep terrain definitions may cause severe errors.

IV.2 Future Work

The comments in the Matlab code and this document will support further development of RPPT. The possible improvements to the program could be as follows;

- Additional antenna patterns and duct models could be defined. Ground and atmospheric parameters defined within the Matlab code could be changed after modifying the user interface. The importation of the terrain profile from a standard digital dataset can be easily implemented.
- More checks should be done for inappropriate input parameters while using RPPT.
- RPPT could be reimplemented in C++ to decrease the execution time.
- Comparisons between RPPT and measured data should be made for increasing the reliability of the program.
- Three dimensional PWE algorithms can be implemented for scattering applications. A hybrid model can be developed by combining ray optics and parabolic equation methods. Hybrid techniques can produce a solution at all angles and heights of interest.
- Range-marching algorithm can be run from the target to the radar. Thus, reflections from the target can be calculated by marching twice.

REFERENCES

[1] Fock, V.A., 1946. *"Solution of the Problem of Propagation of Electromagnetic Waves Along the Earth's Surface by Method of Parabolic Equations"* J. Phys. USSR 10, pp. 13-35.

[2] Tappert, F.D., 1977. *"The Parabolic Approximation Method"*, in Wave Propagation and Underwater Acoustics" chap. 5, edited by J.B. Keller and J.S. Papadakis,New York, Springer-Verlag, vol. 70, pp. 224-287.

[3] Beilis, A., and Tappert, F.D., September 1979. *"Coupled Mode Analysis Of Multiple Rough Surface Scattering"* J. Acoust. Soc. Amer., vol. 66, no. 3, pp. 811-826.

[4] Dozier, L.B., 1984. *"PERUSE : A Numerical Treatment Of Rough Surface Scattering For The Parabolic Wave Equation"* J. Acoust. Soc. Amer., vol. 75, pp. 1415-1432.

[5] Kuttler, J.R., and Dockery, G.D., March-April 1991. *"Theoretical Description Of The Parabolic Approximation / Fourier Split-Step Method Of Representing Electromagnetic Propagation In The Troposphere"* Radio Sci., vol. 26, pp. 381-393.

[6] Dockery, G.D., and Kuttler, J.R., March–April 1996. *"An Improved Impedance–Boundary Algorithm For Fourier Split–Step Solutions Of The Parabolic Wave Equation"* IEEE Trans. Antennas Propagat., vol. 44, pp. 1592-1599.

[7] Barrios, A.E., January 1994. *"A Terrain Parabolic Equation Model For Propagation In The Troposphere"* IEEE Trans. Antennas Propagat., vol. 42, no. 1, pp. 90-98.

[8] *"Software Design Description For The Advanced Propagation Model CSCI (Version 1.0)"* Space and Naval Warfare Systems Center

[9] Mcarthur, R.J., 1992. *"Propagation Modelling Over Irregular Terrain Using The Split–Step Parabolic Equation Method"* Inst. Elect. Eng. Proc. Radar, pp. 54-57.

[10] Levy, M.F., 1997. *"Transparent Boundary Conditions For Parabolic Equation Solutions Of Radiowave Propagation Problems"* IEEE Trans. Antennas Propagat., vol. 45, pp. 66-72.

[11] Janaswamy, R., and Andersen, J.B. , March 2000. *"Path Loss Predictions In Urban Areas With Irregular Terrain Topography"* Wireless Personal Communications, vol. 12, pp. 874-878.

[12] Herbert V. Hitney, August 1994. *"Modelling Surface Effects with the Parabolic Equation Method"* IGARSS'94, pp. 2322-2325.

[13] Donuhue, D.J., and Kuttler, J.R., February 2000. *"Propagation Modelling Over Terrain Using The Parabolic Wave Equation"* IEEE Trans. Antennas Propagat., vol. 48, no. 2, pp. 260-277.

[14] Levy, M., 2000. *Parabolic Equation Methods For Electromagnetic Wave Equation* , Institution Of Electrical Engineers.

[15] Sevgi, L., and Akleman, F., and Felsen, L.B., September 2000. *"Ground Wave Propagaion Modelling : Problem–Matched Analytical Formulations And Direct Numerical Techniques"* IEEE Antennas Propagat. Magazine, pp. 55-75.

[16] Dockery, G.D., 1988. *"Modelling Electromagnetic Wave Propagation In the Troposphere Using The Parabolic Equation"* IEEE Trans. Antennas Propagat., vol. 36, pp. 1464-1470.

[17] Rino, C.L., and Ngo, H.D., 1997. *"Forward Propagation In A Half–Space With An Irregular Boundary"* IEEE Trans. Antennas Propagat., vol. 45, pp. 1340-1347.

[18] Craig, K.H., and Levy, M.F., 1991. *"Parabolic Equation Modelling Of The Effects Of Multipath And Ducting On Radar Systems"* IEE Proc., part F, vol. 138, pp. 153-162.

[19] Smith, K.B., and Tappert, F.D., May 1993. *"UMPE : The University Of Miami Parabolic Equation Model Version 1.1"* MPL Technical Memorandum 432.

[20] Şengül, O., June 2001. *Low Altitude Radar Simulation Program RADCAL*, MSc. Thesis, Dept. of Electrical and Electronic Eng., Middle East Technical University.

[21] Kuttler, J.R., July 1999. *"Differences Between The Narrow–Angle And Wide–Angle Propagators In The Split-Step Fourier Solution Of The Parabolic Wave Equation"* IEEE Trans. Antennas Propagat., vol. 47, no. 7, pp. 1131-1140.

[22] Janaswamy, R., 1998. *"A Curvilinear Coordinate Based Split–Step Parabolic Equation Method For Propagation Predictions Over Terrain"* IEEE Trans. Antennas Propagat., pp. 1-10.

[23] Peter Gerstoft, Donald F. Gingras, 1999. *"Source And Environmental Parameter Estimation Using Electromagnetic Matched Field Processing"* IEEE Proc. ICASSP-99.

[24] Barrios, A.E., July 1992. *"Parabolic Equation Modelling in Horizontally Inhomogeneous Environments"*, IEEE Trans. Antennas Propagat., vol. 40, no. 7, pp. 791-797.

[25] Barrios, A.E., October 1992. *"Terrain Modelling Using The Split Step Parabolic Equation Method"* IEE Radar 92 Int'l Conf., pp. 66-69.

[26] Hitney, H.V., 1992. *"Hybrid Ray Optics And Parabolic Equation Methods For Radar Propagation Modelling"* IEE Proceedings, no. 365, pp. 58-61.

[27] Ayasli, S., 1985. *"SEKE: A Computer Model For Low Altitude Radar Propagation Over Irregular Terrain"* MIT/Lincoln Lab. Project Rep., pp. 1013-1023.

[28] Levy, M.F., and Zaporozhets, 1999. A.A., *"Bistatic RCS Calculations With The Vector Parabolic Equation Method"* IEEE Trans. Antennas Propagat., vol. 47, pp. 1688-1696.

[29] Bebbington, D.H.O., *"An Improved Split–Step Technique For Numerical Modelling Of Propagation In The Troposphere"* pp. 832-835.

[30] Akleman, F., and Sevgi, L., *"Time And Frequency Domain Wave Propagators"* pp. 1-26.

[31] Tappert, F.D., Lee, D., December 1984. *"A Range Refraction Parabolic Equation"* J. Acoust. Soc. Amer., vol. 76, pp. 1797-1803.

[32] Thomson, D.J., and Chapman, N.R., 1983. *"A Wide–Angle Split–Step Algorithm For The Parabolic Equation"* J. Acoust. Soc. Amer., vol. 74, pp. 1848-1854.

[33] Kuttler, J.R., and Huffaker, J.D., 1994. *"Solving The Parabolic Wave Equation With A Rough Surface Boundary Condition"* J. Acoust. Soc. Amer., vol. 94, pp. 2451-2453.

[34] Abarbanel, H.D.I., *"Scattering From A Random Surface"* pp. 1459-1466.

[35] Kuttler, J.R., and Janaswamy, R., 2002. *"Improved Fourier Transform Methods For Solving The Parabolic Wave Equation"* Radio Sci., vol. 37, no. 2, pp. 5.1-5.11.

[36] Merrill I. Skolnik, 1981. *Introduction To Radar Systems*, McGraw-Hill Book Company.

[37] M. Dolukhanov, 1971. *Propagation Of Radio Waves,* Mir Publishers.

[38] Huizing, A. G. and Theil, A., 1993. *CARPET Computer–Aided Radar Performance Evaluation Tool*, Artech House.

[39] Blake, L. V., 1986. *Radar Range Performance Analysis*, Artech House.

APPENDIX A

PROPAGATION FACTOR AND PATH LOSS

The propagation factor is defined as the ratio of the actual electric field at some point to the field that would exist at that point under free-space propagation conditions. Free-space propagation is the propagation of energy that would occur if an omnidirectional point-radiating source were placed in outer space. Propagation Factor for horizontal polarization

$$F_H = \frac{|E|}{|E_0|} = \frac{|E_\phi|}{|E_0|} = |u(x,z)| \sqrt{x\lambda} \tag{A.1}$$

Propagation Factor for vertical polarization

$$F_V = \frac{|H|}{|H_0|} = \frac{|H_\phi|}{|H_0|} = |u(x,z)| Z_0 \sqrt{x\lambda} \tag{A.2}$$

where $Z_0 = 120\pi$. And path loss $L_p(x,z)$ is given by

$$L_p(x,z) = \left(\frac{4\pi x}{\lambda}\right)^2 \times \frac{1}{F^2} \tag{A.3}$$

The effects of propagation from target type, cross-section and radar detection thresholds can be easily included to the path loss.

APPENDIX B

FFT PARAMETERS

After the determination of $z_{\max}$, $p_{\max}$ is found from the Nyquist sampling criterion: $z_{\max} p_{\max} = \pi N_{\text{fft}}$, with N_{fft} being the transform size. The FFT size N_{fft}, is an integer power 2.

The range step $\triangle z$, is computed by

$$\triangle z = \frac{z_{\max}}{N_{\text{fft}}} \tag{B.1}$$

The range step $\triangle x$, is computed by

$$\triangle x = 2k \left(\triangle z\right)^2 \tag{B.2}$$

Fourier shift theorems are used to vary the antenna height and to squint the antenna boresight in the vertical plane.

APPENDIX C

SOURCE MODELLING

The Fourier split-step algorithm requires the initial field $u(0, z)$, in order to propagate the field forward. Fourier transform theory can be used to provide the initial field which will result in the proper antenna pattern shape, beam pointing angle and antenna height, [7, 18, 16, 19]. The antenna pattern can be defined analytically or numerically by considering the maximum propagation angle and FFT size. The far field antenna pattern $F(p)$ and its aperture distribution $f(z)$ are a Fourier transform pair. In the simulation, Omni and Gaussian antenna patterns are handled.

Truncated omnidirectional antenna pattern; $F(p) = 1$ and $f(z) = \delta(z - z_0)$.

Normalized Gaussian antenna pattern;

$$\begin{aligned} F(p) &= Ae^{-\frac{(p-p_0)^2 w^2}{4}} \\ f(z) &= \frac{A}{w\sqrt{\pi}} e^{-\frac{(z-z_0)^2}{w^2}} e^{jp_0 z} \end{aligned} \tag{C.1}$$

where

$$w = \frac{\sqrt{2\ln 2}}{k \sin\left(\frac{\theta_{BW}}{2}\right)}. \tag{C.2}$$

Here, θ_{BW} is the 3 dB beamwidth, $p_0 = k\sin(\theta_0)$ where θ_0 is the beam pointing angle, z_0 is the antenna height and A is the normalization constant ($A = 1$ is used).

APPENDIX D

TERRAIN FUNCTIONS

In the simulation, rectangle hill, sinuson hill, pyramid hill and sinusoidal terrain functions are handled. The first order x-derivative of the terrain function is evaluated by the forward finite-difference approximation and second order x-derivatives of the terrain function is evaluated by the central finite-difference approximation.

$$\begin{aligned} \frac{\partial T\left(x_i\right)}{\partial x} &\cong \frac{T\left(x_{i+1}\right)-T\left(x_i\right)}{\Delta x} \\ \frac{\partial^2 T\left(x_i\right)}{\partial x^2} &\cong \frac{T\left(x_{i+1}\right)+T\left(x_{i-1}\right)-2T\left(x_i\right)}{\Delta x^2}. \end{aligned} \tag{D.1}$$

D.1 Rectangle Hill

$$T(x)=\begin{cases} H_{\text{hill}} & , \ x_1 \leq x \leq x_1+W_{\text{hill}} \\ 0 & , \ \text{elsewhere} \end{cases} . \tag{D.2}$$

In the terrain function $T(x)$, H_{hill} represents the height of the hill and W_{hill} represents the width of the hill.

D.2 Pyramid Hill

$$T(x)=\begin{cases} H_{\text{hill}}\frac{(x-x_1)}{W_{\text{hill}}} & , \ x_1 \leq x \leq x_1+W_{\text{hill}} \\ H_{\text{hill}}\frac{(x_1+2W_{\text{hill}}-x)}{W_{\text{hill}}} & , \ x_1+W_{\text{hill}} \leq x \leq x_1+2W_{\text{hill}} \\ 0 & , \ \text{elsewhere} \end{cases} . \tag{D.3}$$

In the terrain function $T(x)$, H_{hill} represents the height of the hill and $2W_{\text{hill}}$ represents the width of the hill, [13].

D.3 Sinuson Hill

$$T(x) = \begin{cases} \frac{H_{\text{hill}}}{2}\left[1 + \sin\left(\frac{\pi(x-x_1)}{2W_{\text{hill}}}\right)\right] & , \; x_1 - W_{\text{hill}} \leq x \leq x_1 + 3W_{\text{hill}} \\ 0 & , \; \text{elsewhere} \end{cases} . \tag{D.4}$$

In the terrain function $T(x)$, H_{hill} represents the height of the hill and $4W_{\text{hill}}$ represents the width of the hill, [13].

D.4 Sinusoidal Surface

$$T(x) = H_{\text{hill}} \sin(\frac{2\pi x}{\Lambda}) \tag{D.5}$$

In the terrain function $T(x)$, H_{hill} represents the height of the hill and Λ represents the period of the sinusoid, [21, 17].

APPENDIX E

REFRACTIVITY PROFILES

In the simulation, constant, linear, surface layer and elevated layer refractivity profiles are handled.

The refractive index is given by the Debye formula,

$$n = 1 + 77.6 \times 10^{-6} \frac{P}{T} + 0.373 \frac{e}{T^2} \tag{E.1}$$

where P is atmospheric pressure in millibars, T is the temperature in Kelvin, and e is the water vapor pressure in millibars. The refractive index n of the troposphere at the surface of the earth is very close to unity and rarely exceed 1.0004. Therefore, it is customary to use refractivity, N, defined by

$$N = (n - 1) \times 10^6 \tag{E.2}$$

The refractivity N is dimensionless and is expressed in N units. The gradient of the refractive index, $\frac{\partial N}{\partial z}$, within the standard troposphere is approximated as constant by using linear approximation, [14], and is defined as

$$\frac{\partial N}{\partial z} = -40 \ N \text{ units/km} \ . \tag{E.3}$$

The modified index of refraction , $m(z)$, which accounts for earth's curvature, is defined by

$$m\,(z) = n(z) + \frac{z}{a} \tag{E.4}$$

where a is the earth's radius ($a = 6370$ km).

The modified refractivity, M, is defined by

$$M(z) = \left[n - 1 + \frac{z}{a}\right] \times 10^6 \equiv N(z) + 157z \tag{E.5}$$

The modified refractivity M is dimensionless and is expressed in M units. The gradient of the refractive index, $\frac{\partial M}{\partial z}$, within the standard troposphere remains constant, [22, 15], and is defined as

$$\frac{\partial M}{\partial z} = \frac{\partial N}{\partial z} + 157 = 117 \ M \text{ units/km} \tag{E.6}$$

For homogeneous medium ;

$$N(z) = N_0 \tag{E.7}$$

where N_0 can be typically ($N_0 = 340$ N units) or ($N_0 = 325$ N units).

For linear-square refractivity profile ;

$$N(z) = N_0 - \frac{\partial N}{\partial z} z \tag{E.8}$$

where $\frac{\partial N}{\partial z}$ can be typically $\left(\frac{\partial N}{\partial z} = -40 \ N \text{ units/km}\right)$ for standard troposphere.

The maximum wavelength that can be propagated in a surface duct of height h_d is given by

$$\lambda_{\max} = 2.5 \left(\frac{\partial n}{\partial z}\right)^{1/2} h_d^{3/2} \tag{E.9}$$

where $\lambda_{\max}$, z and h_d are in the same units, [36]. Assuming $\left(\frac{\partial n}{\partial z} = 1.57 \times 10^{-7} \ m^{-1}\right)$, at 3 GHz h_d must be at least 22 m, at 1 GHz h_d must be at least 45 m, at 300 MHz h_d must be at least 100 m, at 100 MHz h_d must be at least 210 m. Extended range propagation usually takes place at the higher microwave frequencies due to low surface duct.

E.1 Evaporation Duct

An evaporation duct can be expressed by a log-linear profile, [14]. The modified refractivity profile for evaporation duct can be expressed as

$$M(z) = M(0) + 0.125 \times \left[z - h_d \log\left(\frac{z}{z_0}\right)\right] \tag{E.10}$$

where h_d is the evaporation duct height and z_0 is the roughness length. A typical value for z_0 is $z_0 = 1.5 \times 10^{-4}$ m which is very small.

E.2 Surface Based Duct

A surface based duct can be defined by a bilinear profile or a tri-linear profile. The modified refractivity profile for surface based duct can be expressed as

$$M(z) = \begin{cases} M(0) + \frac{\partial M_1}{\partial z} z & , z \leq h_d \\ M(h_d) + \frac{\partial M_2}{\partial z} z & , h_d < z \end{cases} \tag{E.11}$$

where $\frac{\partial M_1}{\partial z} < 0$, $\frac{\partial M_2}{\partial z} > 0$ and constant. The duct height, h_d, is typically $10 < h_d < 500$ m.

E.3 Elevated Duct

In a stable atmospheric condition, when temperature inversion takes place and a sufficient amount of water vapor is trapped below this inversion, elevated ducts occur. An elevated duct can be defined by a tri-linear profile. For a tri-linear refractivity profile, there exists three parameters ; base height (h_b), thickness and M-deficit ($\Delta M = M(h_b) - M(h_d)$) [23]. The modified refractivity profile for elevated duct can be expressed as

$$M(z) = \begin{cases} M(0) + \frac{\partial M_1}{\partial z} z & , z \leq h_b \\ M(h_b) + \frac{\partial M_2}{\partial z} z & , h_b < z \leq h_d \\ M(h_d) + \frac{\partial M_3}{\partial z} z & , h_d < z \end{cases} \tag{E.12}$$

where $\frac{\partial M_1}{\partial z} > 0$, $\frac{\partial M_2}{\partial z} < 0$, $\frac{\partial M_3}{\partial z} > 0$ and constant.

E.4 Earth Flattening Transformation

The Earth flatting transformation is

$$\begin{aligned} x &= a\theta \\ z &= a \log\left(1 + \frac{h}{a}\right) \end{aligned} \tag{E.13}$$

where a is the Earth's radius and h is the height above the Earth's surface. A height coordinate z which is a logarithmic function of altitude h is used to obtain a conformal transformation. Assuming small h, compared to Earth's radius, we

obtain $z \approx h$. So for low altitudes ($h \leq 5$km) and short ranges ($x \leq 500$km), the modified index of refraction, $m(x, z)$, which accounts for earth's curvature, is defined by

$$m\,(x, z) = n(x, z)(1 + \frac{z}{a}). \tag{E.14}$$